MOUNTAIN-PLAINS CONSORTIUM

MPC 15-303 | J. Kim

Fire Performance of Bridge Members Retrofitted with Near-surface-mounted Carbon Fiber Reinforced Polymer Composites

MPC
MOUNTAIN-PLAINS CONSORTIUM

A University Transportation Center sponsored by the U.S. Department of Transportation serving the Mountain-Plains Region. Consortium members:

Colorado State University
North Dakota State University
South Dakota State University
University of Colorado Denver
University of Denver
University of Utah
Utah State University
University of Wyoming

Fire Performance of Bridge Members Retrofitted with Near-surface-mounted Carbon Fiber Reinforced Polymer Composites

PI: Yail Jimmy Kim, Ph.D., P.Eng., FACI

Department of Civil Engineering
University of Colorado Denver
Denver, Colorado

December 2015

Acknowledgments

The principal investigator gratefully acknowledges all individuals who contributed to the present research report.

Disclaimer

EXECUTIVE SUMMARY

This report presents a two-phase research program studying: (1) the interfacial response of near-surface-mounted (NSM) carbon fiber reinforced polymer (CFRP) strips embedded along a concrete substrate at elevated temperatures, and (2) the behavior of NSM CFRP strips for strengthening concrete members subjected to thermomechanical distress (thermal and mechanical loads are applied simultaneously).

First phase: two types of bonding agents are used: ordinary and high-temperature epoxies. Residual behavior of the interface, including the characteristics of individual constitutive materials, is examined when subjected to a temperature range varying from 25°C [77°F] to 200°C [392°F]. Test results reveal that residual strength of the concrete and CFRP is not influenced by thermal exposure; however, residual strength of the adhesive is affected. The performance of the interface bonded with ordinary epoxy is better than that of the high-temperature one without thermal distress. The latter becomes superior to the former with an increase in temperature. Interaction between the adhesive and concrete controls interfacial capacity and corresponding failure mode, rather than the individual strength of the materials. Probability-based simulation that complements limitation of the experimental investigation, in terms of sample numbers, was conducted to develop design factors.

Second phase: the focus of this research lies in examining temperature-dependent interfacial responses that control the performance of such a CFRP-strengthening system. An experimental investigation was conducted to study various technical aspects associated with the thermal relaxation, heat conduction, load-carrying capacity, failure mode, and damage characterization of the NSM CFRP-concrete interface. Analytical approaches were entailed to generate practical information that can promote use of CFRP-strengthening technologies, based on the two-parameter Weibull function and probability-based capacity simulation. The thermal relaxation of a polymeric bonding agent influenced the transfer of interfacial stresses, including the stress-decrease response time of the interface with temperature. Transient heat flow was apparent across the interface until the strengthening system failed due to the thermomechanical load. The failure plane of the interface was controlled by progression of heat energy in conjunction with the phase transition of the adhesive. The slip of the interface articulated a thermal hysteresis mechanism, when loaded cyclically. The characteristic parameters proposed aided the design of NSM CFRP systems exposed to elevated temperatures.

TABLE OF CONTENTS

LIST OF TABLES

PART I

PART II

LIST OF FIGURES

PART I

PART II

PART I: INTERFACE BETWEEN NEAR-SURFACE-MOUNTED CFRP AND CONCRETE IN THERMAL DISTRESS

1. INTRODUCTION

Structural strengthening with external reinforcement is a proven technology when enhancing the performance of existing reinforced concrete members. Steel-plating, which preceded the use of carbon fiber reinforced polymer (CFRP) composites,[1] provides a technical rationale to the strengthening method. CFRP is a promising material that has a number of benefits (e.g., light weight, high strength and modulus, resistance to fatigue, and ease of application). CFRP plates or laminates can be bonded to the tensile soffit of a constructed reinforced concrete beam using an adhesive. This externally-bonded CFRP technique has been employed for several decades from laboratory to site.[2] Continued research endeavors resulted in another type of strengthening method called near-surface-mounted (NSM) The definition of CFRP technique follows: narrow grooves are precut along a concrete member and CFRP strips or bars are inserted and permanently positioned with a bonding agent. When compared to externally-bonded CFRP, NSM CFRP can better use the strength of CFRP due to improved bond.[3] Literature notes that the concept of NSM was introduced in 1949, while its application with CFRP has only recently been implemented.[4] Provided that NSM CFRP is a relatively new strengthening method in the rehabilitation community and that existing research is primarily dedicated to load-bearing capacity and fundamental bond-slip mechanisms,[5,6] there extensive research still needs to promote this promising technique to the end-user sector, including design aspects.

One of the critical gaps in state-of-the-art research is the behavior of NSM CFRP when subjected to extreme service conditions, such as fire. The needs, in examining the performance of NSM CFRP-strengthened concrete members subjected to a fire, were recently substantiated. Burke et al.[7] tested one way-slabs strengthened with NSM CFRP strips at elevated temperatures (21°C [70°F], 100°C [212°F], and 200°C [392°F]), based on a silicon rubber heating pad. Two distinct types of bonding agents were used: epoxy and cementitious adhesives. The behavior of NSM-CFRP strengthened slabs also was compared to externally-bonded CFRP counterparts. Cementitous adhesives entailed noticeable debonding failure in comparison to epoxy adhesives, whereas the thermal performance of the former was superior to that of the latter. Further research was recommended to understand a relationship between the adhesive characteristics and the load-bearing capacity of NSM CFRP subjected to high temperature, especially when exceeding the glass transition temperature of the adhesive. Kodur and Yu[8] modeled the flexure of reinforced concrete beams retrofitted with NSM CFRP in a fire, based on a macro-scale finite element method. The following temperature-related parameters were taken into consideration: constitutive material responses, bond deterioration, and variable boundary conditions. The model developed was validated against published literature and used for a numerical parametric study. The efficacy of NSM CFRP was dependent on the location of CFRP and type of insulation. Palmieri et al.[9] studied the behavior of full-scale reinforced concrete beams (L = 3.15 m [10 ft]) strengthened with NSM CFRP exposed to a fire for one hour, including in-fire and post-fire responses. To simulate an in-situ service condition, the strengthened beams were preloaded and thermal load was applied. The effectiveness of insulation was discussed in terms of delaying heat transfer to the CFRP system (the highest temperature transferred to the epoxy layer was 130°C

[266°F]). Residual capacity of the conditioned beams having NSM FRP was up to 92% of the control beam.

The aforementioned research programs clarified the global behavior of concrete members strengthened with NSM CFRP at elevated temperatures; however, thermal responses at a CFRP-concrete interface level are not fully elucidated, including the interaction of constituent materials. Most importantly, design recommendations regarding the interface design of NSM CFRP exposed to elevated temperatures are not available. In this paper, an experimental program is used to explain the residual behavior of NSM CFRP-concrete interface subjected to thermally-induced distress, and is followed by performance reliability investigations. Ancillary tests were conducted to measure thermal response of materials associated with the interface. Strength reduction factors with various safety levels were proposed to facilitate the promising strengthening method.

2. RESEARCH SIGNIFICANCE

A number of research papers have been published regarding the failure characteristics of NSM CFRP-concrete interface based on laboratory observations and mechanics-based analytical models.[4] However, there is limited research on durability aspects of NSM CFRP, and corresponding behavior is not sufficiently understood. ACI440.2R-08[10] states basic requirements for strengthening design, in terms of nominal load-bearing capacity subjected to a fire. However, specific design factors are not available, such as those for strength resistance for CFRP-strengthened structures dedicated to structural fire. This fact indicates that practitioners may follow the design information established for conventional structures in a fire, which could lead to significant uncertainty when it comes to CFRP application. It also is unclear in the ACI440.2R-08 document which temperature range is tolerable, in regard to structural performance at elevated temperatures and how the CFRP-concrete interface interacts with thermal load. Although several parameters influence behavior of the NSM CFRP-concrete interface (e.g., groove size, embedment depth, concrete strength and the like[11]), the most important factor at elevated temperatures is the type of adhesive that controls performance of the interface. The polymer-based bond is intrinsically susceptible to thermal distress, which can cause alterations in the morphology and engineering properties of the adhesive. Overall, attention must be given to the interfacial behavior of NSM CFRP, where major stress transfer is achieved between the hosting concrete substrate and the embedded CFRP (i.e., strengthening efficacy relies on the degree of bond between the concrete and the NSM CFRP). Understanding the post-fire performance of constructed facilities is as important as understanding in-fire behavior, because structural members can continuously be used—even after a fire event, if they have been insulated adequately and have not experienced major structural damage. Present research focuses on residual behavior of NSM CFRP-concrete interface bonded with two types of adhesives when subjected to elevated temperatures, and on development of design factors based on probability-based simulation.

3. EXPERIMENTAL PROGRAM

3.1 Materials

Concrete cylinders ($\Phi 100 \times 200$ mm [$\Phi 4 \times 8$ in]) were prepared and tested at 28 days. An average compressive strength of 42 MPa [6,100 psi] was obtained. The CFRP strip (2 mm [0.08 in] thick $\times$16 mm wide [0.63 in]) manufactured with high strength carbon fibers (4,626 MPa [700 ksi]) and a bisphenol epoxy vinyl ester resin has the following material properties according to the manufacturer: tensile strength = 2,068 MPa [300 ksi], tensile modulus = 124 GPa [18,000 ksi], and failure strain = 0.017. To enhance bond between the CFRP and the adhesive, the strip's surface was treated (the retail product had uneven grid-like surfaces on both sides of the strip). Two types of adhesives (i.e., ordinary and high-temperature epoxies) were used to install the NSM CFRP strip inside the concrete substrate. The ordinary epoxy is a typical structural adhesive, consisting of a resin-hardener mixture (the manufacturer of this particular adhesive does not report its engineering properties, however, the properties when embedded in concrete are available). The high-temperature epoxy is designed to preserve thermal stability up to a glass transition temperature of 170°C [338°F], including tensile strength = 213 MPa [31 ksi], tensile modulus = 374 MPa [54 ksi], glass transition temperature = 170°C [338°F], and ultimate strain = 0.016.

3.2 Preparation of Specimens

Given that the failure of an NSM CFRP-strengthened concrete beam occurs in the effective tensile zone [Fig. I.1(a)], its behavior was represented by an isolated element-level interface. Table I.1 details test configuration of 48 interface specimens, including type of adhesive (OE = ordinary epoxy and HE = high-temperature epoxy) and number of repetitions per exposed temperature (to be discussed). Each specimen was comprised of one concrete block (200 mm [8 in] long $\times$ 100 mm [4 in] deep $\times$ 100 mm [4 in] wide) with a longitudinal groove (25 mm [1 in] deep $\times$ 13 mm [0.5 in] wide) in which two precut CFRP strips (16 mm [0.63 in] wide $\times$ 2 mm [0.08 in] thick $\times$ 150 mm [6 in] long, each) were bonded [Fig. I.1(a)]. Groove size was designed in conformance with the provision of ACI.440.2R-08.[10] Prior to bonding the CFRP strips, the adherent surface inside the groove was cleaned using an air brush to remove any unnecessary substance. To preclude premature failure of the interface caused by stress concentrations at the termination of the groove, the strips were not bonded with styrofoam at both ends of the specimen (Fig. I.1). Ancillary test specimens, such as concrete cylinders and adhesive coupons, (12 mm [0.47 in] wide $\times$ 100 mm [4 in] long $\times$ 6 mm [0.24 in] thick) were prepared to measure their thermal responses.

3.3 Test Procedure

3.3.1 Thermal exposure

After curing the interface specimens per manufacturers' recommendation, all test specimens were submitted to elevated temperatures. An electric furnace equipped with a digital temperature adjustment function was used for this purpose. The range of temperature exposure varied from 25°C [77°F] to 200°C [392°F], as listed in Table I.1. Each temperature level was maintained for

three hours, a time period is frequently used for high-temperature-related research in structural concrete. This is because thermal insulation can maintain the temperature of concrete below 200°C [392°F] for three hours during a fire.[12] The preheated temperature was checked with a laser thermometer before conditioning test specimens [Fig. I.2(a)], followed by temperature-monitoring using thermocouple wires [Fig. I.2(b)]. After achieving three hours of thermal exposure, all specimens cooled down to room temperature to perform residual testing. A spontaneous morphological recovery process (i.e., a flexible rubbery state to a glassy hard state) was observed in the adhesives as the thermal load faded.

3.3.2 Dynamic mechanical analysis

Thermal properties of the CFRP and adhesives were characterized by Dynamic Mechanical Analysis (DMA). Following the procedures of ASTM D7028 (*Standard test method for glass transition temperature of polymer matrix composites by dynamic mechanical analysis*),[13] test coupons were prepared and tested (Fig. I.3). Oscillating stresses were applied to the specimen with an increasing temperature, and the response strain was recorded. Because the CFRP and polymeric adhesives had viscoelastic nature, phase-lag in their constitutive relationship was observed. Storage- and loss-moduli were specified and a phase angle (Tan Delta) was obtained by a computerized DMA instrument. The glass transition temperature (T_g) of the materials was determined at individual peak phase angles.

3.3.3 Material-level test

Conditioned concrete cylinders at elevated temperatures were monotonically loaded to failure and their temperature-dependent residual compressive strength was measured [Fig. I.4(a)]. The effect of thermal distress on strength variation of the CFRP and adhesives was quantified according to ASTM D638 (*Standard test method for tensile properties of plastics*)[14] with mechanical-pressure gripping, as shown in Fig. I.4(b) and (c). Loading rate of the concrete test was 2.5 kN/min [0.56 kip/min], while that of the adhesives was 0.1 mm/min [0.004 in/min]. An extensometer was mounted to the coupons to measure strain responses.

3.3.4 Mechanical testing at interface-level

The interface test specimen was mounted to a universal testing machine and monotonically tensioned at a loading rate of 0.1 mm/sec [0.004 in/sec] until failure occurred. To avoid premature concrete-splitting near the middle of the specimen, at which the CFRP termination existed, a custom-made clamping system was used to confine the concrete block [Fig. I.2(c)]. The clamping apparatus consisted of four perforated hollow steel sections (38 mm [1.5 in] × 38 mm [1.5 in]), four threaded rods (9.5 mm [0.38 in] in diameter), and eight fasteners. The rods were snug-tight so unnecessary initial compressive stresses were not transferred to the concrete.

4. TEST RESULTS AND DISCUSSION

4.1 Temperature Effect at Material-level

4.1.1 Thermal characteristics

The DMA result of the CFRP composite is shown in Fig. I.5(a). The storage modulus was maintained up to a temperature of 100°C [212°F] and then gradually reduced. The phase angle indicated as Tan Delta began to increase at 65°C [149°F] and reached a peak value at 136°C [277°F]. This observation illustrates that (1) the matrix resin of the CFRP strip commenced a phase transition from glassy to rubbery states at 65°C [149°F], and (2) the CFRP composite revealed a state change at 136°C [277°F] from a macro-scale view point. It is important to note that the measured glass transition temperature of the CFRP does not necessarily mean a physical alteration in thermal stability of the carbon fibers. Most carbon fibers preserve structural functionality over 1,000°C [1,832°F][15]. Applied mechanical stress to the composite was not adequately transferred to each fiber due to degradation of the matrix material. In the case of thermosetting polymeric adhesives, a sudden drop in storage modulus was observed at 47°C [117°F] and 125°C [257°F] for the ordinary and high temperature epoxies, respectively, and the peak phase angles were observed at 62°C [144°F] and 155°C [311°F], as shown in Fig. I.5(b) and (c).

4.1.2 Residual strength of constituents

Figure I.6(a) exhibits residual strength variation of the concrete after thermal exposure. To highlight the effect of elevated temperatures, individual strength was normalized by the average strength of the concrete at 25°C [77°F]. Strength of other materials shown in Fig. I.6 was normalized in the same manner. Although a propensity for decreasing compressive strength was observed with temperature, thermal distress appeared to be negligible in the temperature range studied. Tensile strength of the CFRP strips was consistent irrespective of elevated temperatures, as shown in Fig. I.6(b). Failure of the strip took place due to rupture of carbon fibers, which implies that tensile strength of the composite was controlled by the fibers, rather than the resin matrix. Therefore, strength was not influenced by thermal effect even though glass transition temperature of the composite was measured at 136°C [277°F]. Unlike the concrete and CFRP cases, adhesive test results resulted in significant scatter [Fig. I.6(c) and (d)]. This may be attributed to the fact that polymeric chains of the adhesives were not uniformly deteriorated at elevated temperatures. This also could be associated with manual mixing in the laboratory (i.e., potentially uncertain homogeneity from a micro-scale point of view). Despite scattered residual stress, several trends in thermal behavior were noticed: average residual strength of the ordinary epoxy tended to augment with an increase in temperature, while that of the high-temperature epoxy remained virtually unchanged (i.e., the normalized average residual stresses varied near unity). These observations may be due to ordinary epoxy undergoing secondary curing, which strengthened the bond of recovered polymeric chains when the epoxy cooled down[16]. Such an effect was not substantiated for the specially-cured high-temperature epoxy (i.e., variable curing temperatures up to 176°C [350°F], per the manufacturer's application guide). It also is believed that amorphous polymeric structures of the ordinary epoxy were altered and reordered with a gradual decrease in temperature.[17]

4.2 Residual Behavior of NSM CFRP-concrete Interface

4.2.1 Interfacial capacity

Ultimate capacity of the interface test specimens is listed in Table I.1, including those bonded with ordinary and high-temperature epoxies (the OE and HE series, respectively). The control strength of the OE specimens at 25°C [77°F] was 20% higher than that of the HE counterparts, while the strength decrease of the former, due to thermal distress, was more significant than that of the latter (e.g., decreases of 90% and 28% were noticed for the OE and HE categories, respectively, when a temperature varied from 25°C [77°F] to 200°C [392°F]). Figure I.7 further explains the temperature-dependent variation of the interfacial capacity. For the OE specimens [Fig. I.7(a)], interfacial strength was essentially maintained up to 75°C [167°F], beyond which a noticeable drop was observed. It is postulated that passing the glass transition temperature of the OE adhesive (62°C [144°F]) caused some degradation in interfacial response between the adhesive and concrete (further details are available in the failure mode section) even though residual strength of the adhesive itself was not reduced, as discussed earlier. A temperature of 175°C [347°F] was the upper limit of the interface from a load-bearing perspective. In other words, the OE-based interface did not function as a structural component when subjected to a temperature higher than 175°C [347°F]. It should be noted that the OE-200-3 specimen prematurely failed during mechanical loading and therefore, its capacity was not reported. The interfacial capacity of the HE specimens is revealed in Fig. I.7(b). Variation of the average capacity was almost linear with temperature, and no abrupt capacity-drop was noticed up to 200°C [392°F]. The HE category [Fig. I.7(b)] showed less capacity variation than the OE category [Fig. I.7(a)]. For instance, the average coefficient of variation of the HE and OE specimens were 0.106 and 0.186, respectively, within a temperature range of 25°C [77°F] to 200°C [392°F].

4.2.2 Performance characterization

A comparative statistical study was conducted using the Analysis of Variance (ANOVA) to examine similarity or dissimilarity between the experimental OE and HE categories from a temperature-susceptibility view point:

$$F = \frac{m\sigma_{\bar{x}}^2}{\left(\sum_{i=1}^{k}\sigma_i^2\right)/k} \tag{I.1}$$

where F is the F distribution of the tested interface; m is the sample size per test group; $\sigma_{\bar{x}}^2$ is the sample variance; σ_i^2 is the sample variance per group; and k is the number of the populations. A critical F distribution value at a 5% level of significance ($F_{.05}$) can be identified by the degree of freedom defined (DOF) as DOF = (k-1,n-k) in which n is the total number of interfacial capacity in all test specimens. The hypotheses tested were:

H_0: all the mean normalized capacities are equal within the performance division
H_0: not all the mean normalized capacities are equal within the performance division

To identify the degree of thermal degradation, interfacial capacity of each test specimen was normalized with the average capacity of the specimens having no thermal distress (i.e., OE-25 and HE-25 series), as shown in Fig. I.8. Table I.2 summarizes details of the statistical analysis for the OE and HE interface categories, depending upon exposure temperature. Although the mean interfacial capacity of the test specimens in normalized capacity (Fig. I.8) was different between 25°C [77°F] and 175°C [347°F], the calculated F distribution values were less than the critical limit ($F_{.05} = 7.71$). This means that there was insufficient statistical evidence to reject the hypothesis H_0 (i.e., the performance of the OE and HE categories was the same from a statistics perspective within these temperature ranges). On the other hand, the F statistic value exceeded the limit $F_{.05}$ at 200°C [392°F], implying the superior performance of the HE-based interface. The above observations reveal that the experimental data were not sufficient to draw meaningful statistical conclusions in terms of interfacial capacity, especially in temperatures below 175°C [347°F], and suggest the need for refined investigations with more statistical data samples to propose design recommendations. This is addressed in the design proposal section.

4.2.3 Load-displacement response

Figure I.9 depicts load-displacement behavior of the interface. Only selected temperatures are shown for clarity. Residual response of the OE specimens [Fig. I.9(a)] was basically linear with a brittle load drop at their peak load, including similar stiffness, except for response of the category exposed to 200°C [392°F], which demonstrated gradual load-softening after the peak load. These results imply that recovery of the residual behavior was reasonably available up to an exposure temperature of 100°C [212°F]. Beyond this temperature, irreversible thermal damage controlled the specimen behavior and a low strength was noticed, particularly significant at 200°C [392°F]. Figure I.9(b) shows that load-displacement behavior of the HE category was not very different from that of the OE category, except for the facts that (1) the HE specimens tended to exhibit more displacement at their peak loads than did the OE specimens, and (2) the response of the HE200 category was close to that of others, which is remarkably different from the case of the OE specimens.

4.2.4 Failure mode

Figure I.10(a) illustrates the interfacial failure of the OE specimen subjected to 50°C [122°F], which represents a typical failure pattern of the specimens within an exposure temperature range between 25°C [77°F] and 50°C [122°F]. The failure took place within the concrete substrate and no evidence of adhesive-damage was observed, except near the CFRP termination point at the middle of the specimen where a geometric discontinuity existed (i.e., the gap between the CFRP strips, Fig. I.1). The adhesion and cohesion capacity of the adhesive was stronger than the cohesion capacity of the concrete. Such a failure trend was, however, altered when exposed to a higher temperature, as shown in Fig. I.10(b). The interfacial failure occurred along the bond line rather than within the concrete substrate. This result shows that the bonding agent was deteriorated because of thermal distress and hence its bonding characteristics weakened and insufficient shear-stress transfer became available from the CFRP to the concrete, which explains

the reduced interfacial capacity discussed in Fig. I.7(a). Given stress redistribution from the NSM CFRP to the surrounding concrete is an important parameter in structural strengthening, this type of failure is not desirable in practice[18]. With an increase in temperature, the failure mode of the OE specimens tended to shift from Fig. I.10(a) to (b). The failure of the HE category was somewhat distinct from that of the OE category. The failure plane was close to the surface of the concrete, including some local splitting of the concrete, irrespective of thermal exposure, as shown in Fig. I.10(c) and (d). This is why the interfacial capacity of the HE specimens was relatively lower than that of the OE specimens (Table I.1) and the capacity reduction of the HE was not as significant as that of the OE at elevated temperatures (Fig. I.7).

5. DESIGN PROPOSAL

5.1 Formulation of Reliability Framework

In most structural designs, one- to four-hour fire ratings can be achieved by selecting adequate insulation material and corresponding thickness.[19] A three-hour rating was adopted for this study in conformance with the experimental investigation. Figure I.11 demonstrates the effect of insulation on retarding heat transfer from a fire to a CFRP-strengthened reinforced concrete slab.[20] The fire temperature applied to the slab was similar to the standard fire temperature of ISO834,[21] whereas significantly lower temperatures were recorded at a CFRP-insulation interface level (designated 'with insulation' in Fig. I.11). According to the variation of the insulated CFRP temperature and the present test data, thermal ranges were refined and five performance categories were proposed accordingly, as illustrated in Fig. I.11. Monte-Carlo simulation was then conducted to generate statistical data based on the fitted equations (Fig. I.7) representing residual capacity of the NSM CFRP-concrete interface at elevated temperatures so the insufficient test data was complemented. The coefficient of variation (COV) in temperature was taken as 0.45.[22] It is worthwhile to note that such a COV is larger than the ones measured in the controlled laboratory (e.g., COV = 0.002 at 100°C [212°F]). Therefore, the design recommendations developed appear to be sufficiently conservative for design and practice. A sensitivity analysis was done to identify an acceptable number of data sampling [Fig. I.12(a)]. Provided the variation of a fire temperature was represented by a normal probability distribution,[23] random data sampling was conducted for the interface subjected to variable temperatures ranging from 25°C [77°F] to 200°C [392°F], as shown in Fig. I.12(b) and (c). The trend of such data sampling was that uncertainty augmented with an increase in temperature (i.e., wider data range). Although the number of test specimens is limited, the sampling range of the Monte-Carlo simulation can effectively address potential uncertainty associated with the interfacial capacity at elevated temperatures. The Three-Sigma Rule,[24] which may be useful for determining statistical parameters when the number of samples is not enough, corroborates such an assertion. The estimated average COV values of the OE- and HE-based interfacial capacities are 0.05 and 0.03, respectively. These magnitudes are considerably less than those used in the present Monte-Carlo simulation [Fig. I.12(b) and (c)].

5.2 Calibration of Resistance Factor

To determine resistance factors for the NSM CFRP-concrete interface subjected to elevated temperatures, an established method was employed:[25, 26]

$$\phi = \lambda\left(1-\alpha\beta COV_R\right) \le 1.0 \tag{I.2}$$

where ϕ is the resistance factor at a temperature T; λ is the bias factor; α is the direction cosine; β is the safety index; and COV_R is the coefficient of variation of the interface at a temperature T obtained from the Monte-Carlo simulation. Three levels of safety indices were examined (β = 2.5, 3.0, and 3.5) to generate practical design recommendations. Given the present investigation did not include an applied load effect, the direction cosine was approximated to be α = 0.79, which is valid for typical structural reliability.[26] The bias factor was set to unity, which would lead to developing of conservative design factors. (Typical bias factors for reinforced concrete

structures are positioned between 1.10 and 1.14;[26] however, accurate bias factors cannot be provided at this time because no predictive models exist on the behavior of NSM CFRP-concrete interface at elevated temperatures). Figure I.13 reveals the temperature-dependent resistance factors of the interface calculated at various safety levels. The factor of the HE-based interface was maintained, whereas that of the OE-based interface showed noticeable drops, in particular, beyond a temperature of 75°C [167°F]. Simulated results of the OE-based interface appeared to be more susceptible to temperature (i.e., noticeable drop in resistance factor with an increasing temperature), whereas their trend was fundamentally in agreement with the test data discussed in Fig. I.7. Table I.3 summarizes all the strength reduction factors associated with specific safety levels, adhesive types, and performance categories. It is expected that the level of safety representing the probability of failure would be dependent on the designer's discretion when conducting a strengthening design.

6. SUMMARY AND CONCLUSISIONS

This paper discussed an experimental investigation into the residual behavior of NSM CFRP-concrete interface at elevated temperatures from 25°C [77°F] to 200°C [392°F]. Two types of bonding agents were used: ordinary and high-temperature epoxies. Ancillary tests were conducted to characterize thermal response of constitutive materials, such as strength and glass transition temperature. To expand laboratory results, which had a relatively insufficient number of test specimens, probability-based simulation was done and corresponding results were employed for developing design factors at various levels of safety. The proposed design factors are valid only when the CFRP-concrete interface is adequately insulated so the effect of thermal exposure is retarded in case of a fire. The behavior of NSM CFRP-concrete interface subjected to simultaneous thermal and mechanical loads must be examined with the residual test results elaborated in this test program, so a complete understanding of this strengthening method at elevated temperatures can be achieved. The following conclusions were drawn:

- The effect of elevated temperatures on the residual strength of concrete and the CFRP was insignificant in the temperature range studied, while they did influence the response of polymeric adhesives. The ordinary epoxy (OE) was more susceptible to thermal load than the high-temperature epoxy (HE).
- The OE-based interface exhibited a 20% higher strength in comparison to the HE-based counterpart without thermal distress; however, the former showed a more noticeable strength decrease than the latter when exposed to elevated temperatures because of irreversible thermal damage established in the interface system.
- Failure of the interface was controlled by interaction between the adhesive and the concrete substrate rather than their material strength. The degree of shear stress transfer (or stress redistribution) between the CFRP and the concrete was temperature-dependent, which was affected by the type of bonding agent. The dominant failure mode of the OE specimens shifted from the concrete side to the adhesive side with an increase in temperature, whereas the failure mode of the HE specimens was consistent regardless of thermal exposure.
- Test data were insufficient to draw meaning statistical comparisons between the OE and HE-specimens at or below a temperature of 175°C [347°F], while the probability-based simulation with a total of 80,000 sample populations clarified the effect of thermal exposure and resulted in strength reduction factors recommended for implementing interface design of the NSM CFRP at elevated temperatures.

7. REFERENCES

[1] Hollaway, L.C. and Leeming, M.B. 1999. Strengthening of reinforced concrete structures, Woodhead Publishing, Cambridge, UK.

[2] Kim, Y.J. 2014. Advanced composites in bridge construction and repair, Woodhead Publishing, Elsevier, Cambridge, UK.

[3] Barros, J.A.O., Baghi, H., Dias, S.J.E., and Ventura-Gouveia, A. 2013. A FEM-based model to predict the behaviour of RC beams shear strengthened according to the NSM technique, Engineering Structures, 56, 1192-1206.

[4] De Lorenzis, L. and Teng, J.G. 2007. Near-surface mounted FRP reinforcement: an emerging technique for strengthening structures, Composites Part B, 38, 119-143.

[5] El-Hacha, R. and Rizkalla, S.H. 2004. Near-surface-mounted fiber-reinforced polymer reinforcements for flexural strengthening of concrete structures, ACI Structural Journal, 101(5), 717-726.

[6] Hassan, T.K. and Rizkalla, S.H. 2004. Bond mechanism of near-surface-mounted fiber-reinforced polymer bars for flexural strengthening of concrete structures, ACI Structural Journal, 101(6), 830-839.

[7] Burke, P.J., Bisby, L.A., and Green, M.F. 2013. Effects of elevated temperature on near surface mounted and externally bonded FRP strengthening systems for concrete, Cement and Concrete Composites, 35, 190-199.

[8] Kodur, V.K.R. and Yu, B. 2013. Evaluating the fire response of concrete beams strengthened with near-surface-mounted FRP reinforcement, Journal of Composites for Construction, 17(4), 517-529.

[9] Palmieri, A., Matthys, S., and Taerwe, L. 2013. Fire endurance and residual strength of insulated concrete beams strengthened with near-surface mounted reinforcement, Journal of Composites for Construction, 17(4), 454-462.

[10] ACI. 2008. Guide for the design and construction of externally bonded FRP systems for strengthening concrete structures (ACI440.2R-08), American Concrete Institute Committee 440, Farmington Hills, MI.

[11] Novidis, D.G. and Pantazopoulou, S.J. 2008. Bond test of short NSM-FRP and steel bar anchorages, Journal of Composites for Construction, 12(3), 323-333.

[12] Kodur, V.K.R., Bisby, L.A., and Green, M.F. 2007. Guidance for the design of FRP-strengthened concrete members exposed to fire, Journal of Fire Protection Engineering, 17(5), 5-26.

[13] ASTM. 2007. Standard test method for glass transition temperature of polymer matrix composites by dynamic mechanical analysis (ASTM D7028-07), American Society for Testing and Materials, West Conshohocken, PA.

[14] ASTM.2010. Standard test method for tensile properties of plastics (ASTM D638-10), American Society for Testing and Materials, West Conshohocken, PA.

[15] Rostasy, F. 1992. Fiber composite elements and techniques as non-metallic reinforcement of concrete, Brite project 4142/BREU-CT910515, Evaluation of Potential and Production Technologies of FRP, Technical Report Task 1.

[16] Moussa, O., Vassilopoulos, A.P., de Castro, J., and Keller, T. 2012. Time-temperature dependence of thermomechanical recovery of cold-curing structural adhesives, International Journal of Adhesion and Adhesives, 35, 94-101.

[17] Hu, W. 2013. Polymer physics, Springer, Berlin, Germany

[18] Seracino, R., Jones, N.M., Ali, M.S.M., Page, M.W., and Oehlers, D.J. 2007. Bond strength of near-surface mounted FRP strip-to-concrete joints, Journal of Composites for Construction, 11(4), 401-409.

[19] PCI. 2010. PCI deign handbook (7^{th} edition), Precast/Prestressed Concrete Institute, Chicago, IL.

[20] Williams, B.K. 2004. Fire performance of FRP-strengthened reinforced concrete flexural members, PhD Thesis, Queen's University, Kingston, ON, Canada.

[21] ISO. 1999. Fire resistance tests-elements of building construction (ISO 834), International Organization for Standardization, Geneva, Switzerland.

[22] Eamon, C.D. and Jensen, E. 2012. Reliability analysis of prestressed concrete beams exposed to fire, Engineering Structures, 43, 69-77.

[23] Hasofer, A.M., Beck, V.R., and Bennetts, I.D. 2007. Risk analysis in building fire safety engineering, Butterworth-Heinemann, Burlington, MA.

[24] Duncan, J.M. 2000. Factors of safety and reliability in geotechnical engineering, Journal of Geotechnical and Geoenvironmental Engineering, 126(4), 307-316.

[25] Ang, A.H.-S. and Tang, W.H. 1984. Probability concepts in engineering planning and design, John Wiley and Sons, New York, NY.

[26] Barker, R.M. and Puckett, J.A. 1997. Design of highway bridges based on AASHTO LRFD bridge design specifications, John Wiley and Sons, New York, NY.

Table I.1 Specimens for NSM CFRP-concrete interface test

Bonded with ordinary epoxy						Bonded with high-temperature epoxy					
ID	P_u (kN [kip])		ID	P_u (kN [kip])		ID	P_u (kN [kip])		ID	P_u (kN [kip])	
	Each	Ave		Each	Ave		Each	Ave		Each	Ave
OE25-1	21.2 [4.8]	21.5 [4.8]	OE125-1	17.5 [3.9]	16.2 [3.6]	HE25-1	16.9 [3.8]	17.2 [3.9]	HE125-1	11.4 [2.6]	12.8 [2.9]
OE25-2	19.1 [4.3]		OE125-2	13.3 [3.0]		HE25-2	16.5 [3.7]		HE125-2	13.4 [3.0]	
OE25-3	24.1 [5.4]		OE125-3	17.6 [4.0]		HE25-3	18.1 [4.1]		HE125-3	13.6 [3.1]	
OE50-1	18.2 [4.1]	20.3 [4.6]	OE150-1	13.4 [3.0]	17.8 [4.0]	HE50-1	16.4 [3.7]	16.1 [3.6]	HE150-1	14.6 [3.3]	15.2 [3.4]
OE50-2	23.3 [5.2]		OE150-2	19.4 [4.4]		HE50-2	16.5 [3.7]		HE150-2	15.9 [3.6]	
OE50-3	19.4 [4.4]		OE150-3	20.6 [4.6]		HE50-3	15.3 [3.4]		HE150-3	15.0 [3.4]	
OE75-1	19.4 [4.4]	20.7 [4.7]	OE175-1	14.6 [3.3]	13.2 [3.0]	HE75-1	12.8 [2.9]	15.1 [3.4]	HE175-1	11.4 [2.6]	13.1 [2.9]
OE75-2	20.7 [4.7]		OE175-2	11.3 [2.5]		HE75-2	14.5 [3.3]		HE175-2	13.0 [2.9]	
OE75-3	21.9 [4.9]		OE175-3	13.9 [3.1]		HE75-3	18.1 [4.1]		HE175-3	15.0 [3.4]	
OE100-1	15.5 [3.5]	17.1 [3.8]	OE200-1	3.1 [0.7]	2.2 [0.5]	HE100-1	16.6 [3.7]	16.3 [3.7]	HE200-1	13.2 [3.0]	12.3 [2.8]
OE100-2	16.6 [3.7]		OE200-2	1.3 [0.3]		HE100-2	18.8 [4.2]		HE200-2	12.2 [2.7]	
OE100-3	19.1 [4.3]		OE200-3	N/A		HE100-3	13.5 [3.0]		HE200-3	11.7 [2.6]	

P_u = ultimate load; N/A = premature failure during test

Table I.2 Analysis of variance (ANOVA) for thermal performance at 5% level of significance

	25°C [77°F]	50°C [122°F]	75°C [167°F]	100°C [212°F]	125°C [257°F]	150°C [302°F]	175°C [347°F]	200°C [392°F]
$\bar{\bar{\mu}}$	1.0	0.94	0.92	0.87	0.75	0.86	0.69	0.41
$\sigma^2_{\bar{x}}$	0.0000	0.0000	0.0033	0.0119	0.0000	0.0015	0.0108	0.1909
F	0.0000	0.0168	0.7000	2.2769	0.0058	0.2618	3.6851	208.4491
$F_{.05}$	7.71	7.71	7.71	7.71	7.71	7.71	7.71	10.13
D	N	N	N	N	N	N	N	R

$\bar{\bar{\mu}}$ = grand mean; $\sigma^2_{\bar{x}}$ = Sample variance; F = F statistic; $F_{.05}$ = Critical limit; D = Decision (N: *Do not reject* H_0 and R: *reject* H_0)

Table I.3 Proposed strength reduction factor up to 3-hr fire rating

Reduction factor	Safety level	Failure probability	Performance category				
			1	2	3	4	5
ϕ (OE)	β = 2.5	0.62×10^{-2}	0.85	0.75	0.55	N/A	N/A
	β = 3.0	1.35×10^{-3}	0.80	0.70	0.50	N/A	N/A
	β = 3.5	2.33×10^{-4}	0.80	0.65	0.40	N/A	N/A
ϕ (HE)	β = 2.5	0.62×10^{-2}	0.95	0.90	0.90	0.90	0.80
	β = 3.0	1.35×10^{-3}	0.95	0.90	0.90	0.90	0.75
	β = 3.5	2.33×10^{-4}	0.90	0.90	0.90	0.85	0.70

OE = ordinary epoxy; HE = high-temperature epoxy; N/A = not applicable

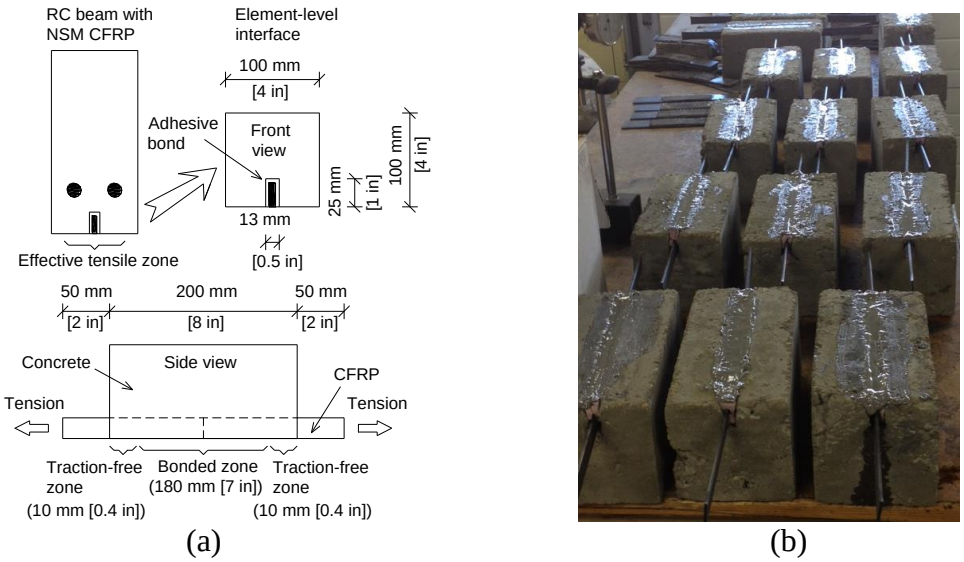

Fig. I.1 Interface test specimen: (a) dimension (not to scale), (b) prepared specimens

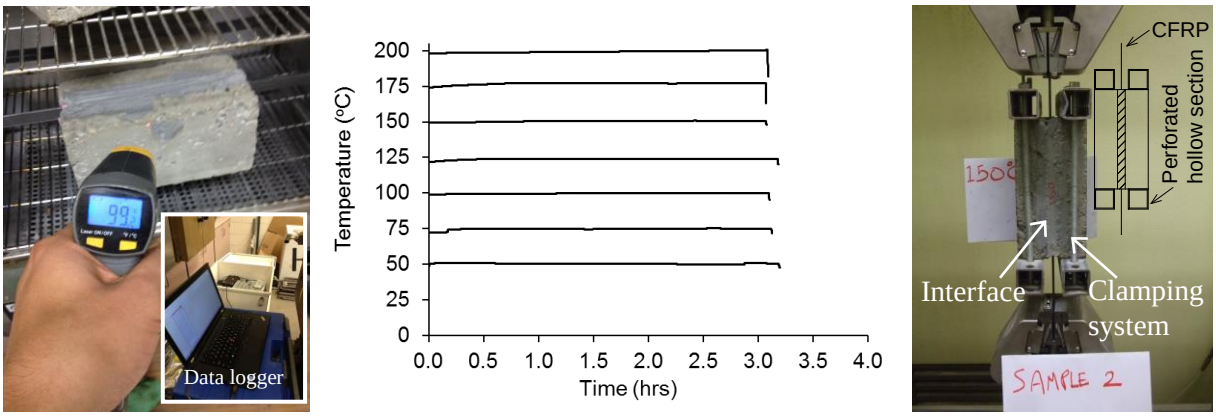

(a) (b) (c)

[°F = (°C × 1.8) + 32]

Fig. I.2 Test scheme for NSM CFRP-concrete interface: (a) thermal exposure, (b) temperature variation, (c) mechanical loading

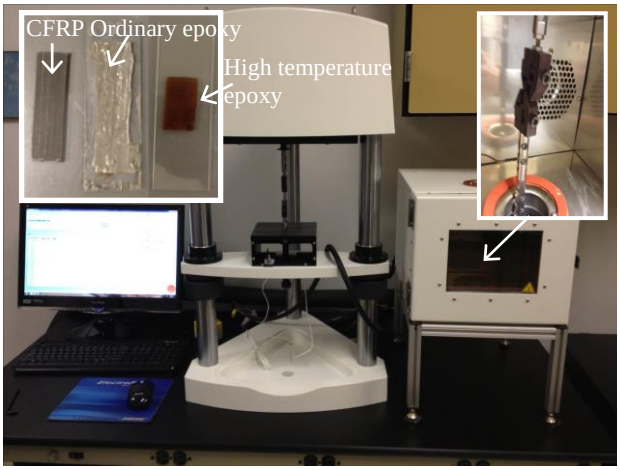

Fig. I.3 Dynamic mechanical analysis (DMA)

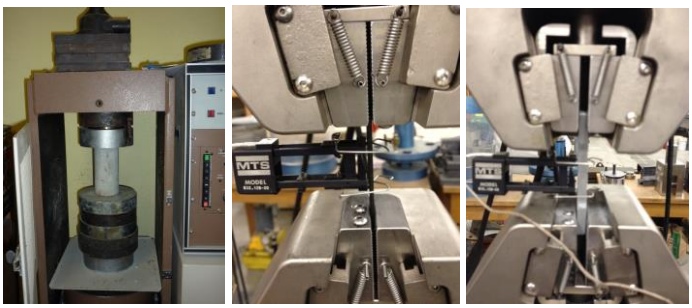

(a) (b) (c)

Fig. I.4 Material-level test: (a) concrete, (b) CFRP strip, (c) adhesive

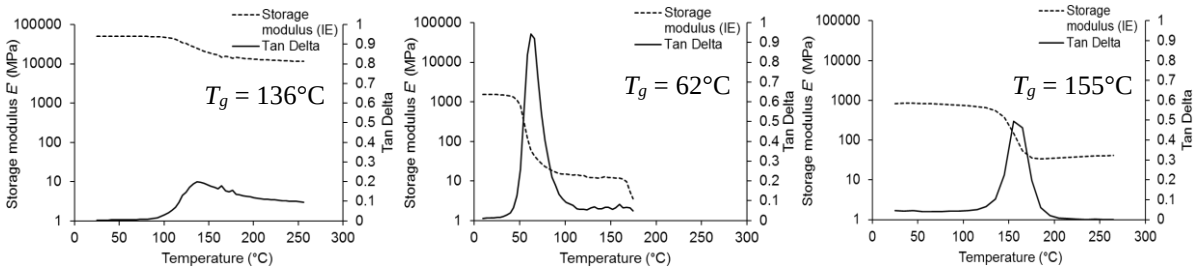

[1 MPa = 145 psi; °F = (°C × 1.8) + 32]

Fig. I.5 Dynamic mechanical analysis (DMA) results: (a) CFRP strip, (b) ordinary epoxy, (c) high-temperature epoxy

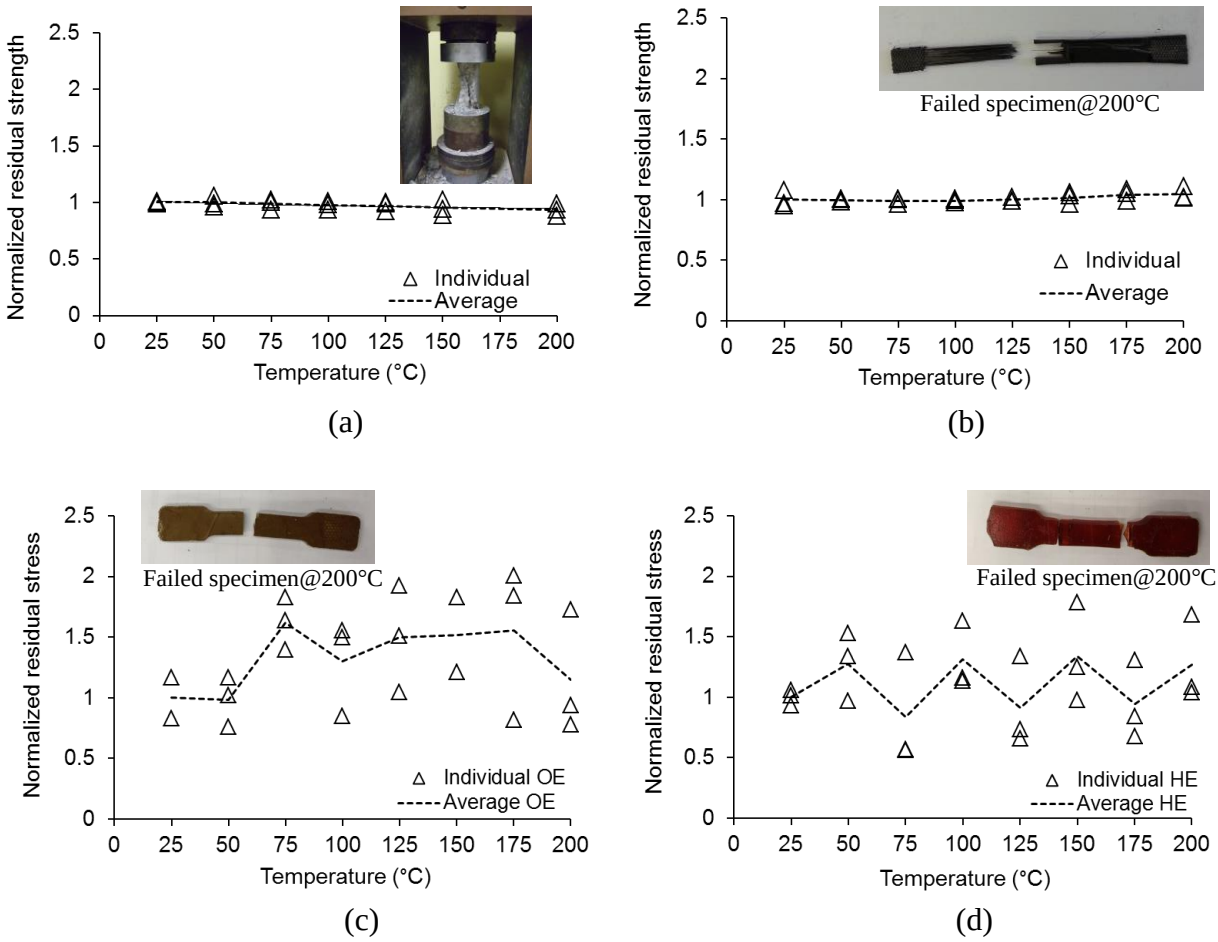

[°F = (°C × 1.8) + 32]

Fig. I.6 Temperature-dependent strength variation: (a) concrete in compression, (b) CFRP strip in tension, (c) ordinary epoxy in tension, (d) high-temperature epoxy in tension

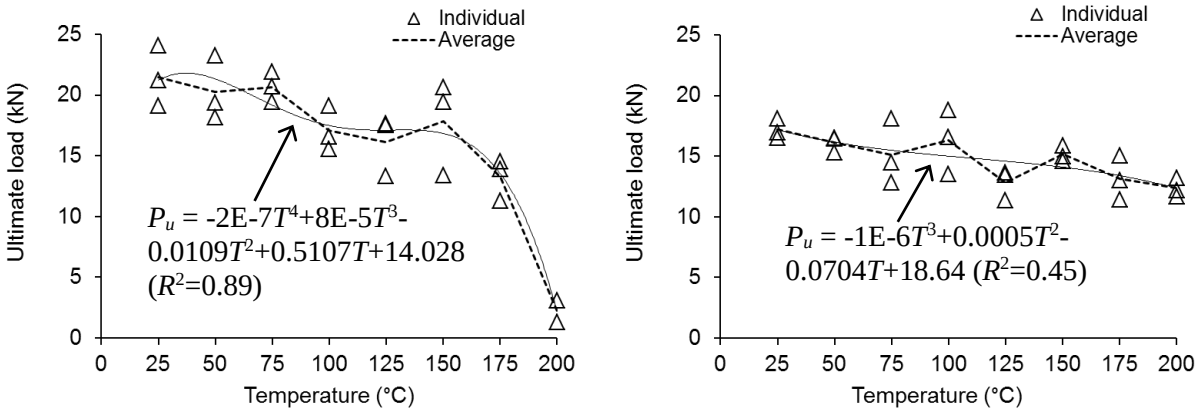

(a) (b)

[1 kN = 0.225 kip; °F = (°C × 1.8) + 32]

Fig. I.7 Temperature-dependent interfacial strength: (a) specimens bonded with ordinary epoxy, (b) specimens bonded with high-temperature epoxy

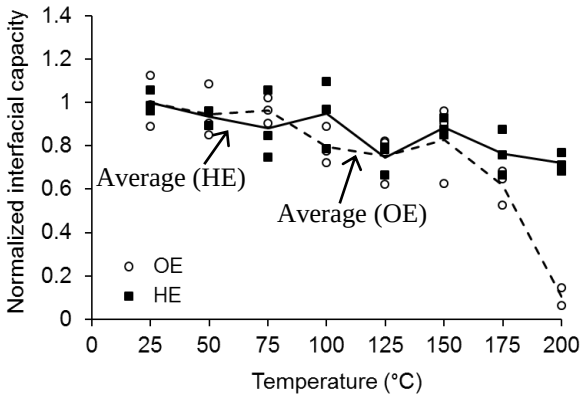

Fig. I.8 Normalized comparison of interfacial capacity

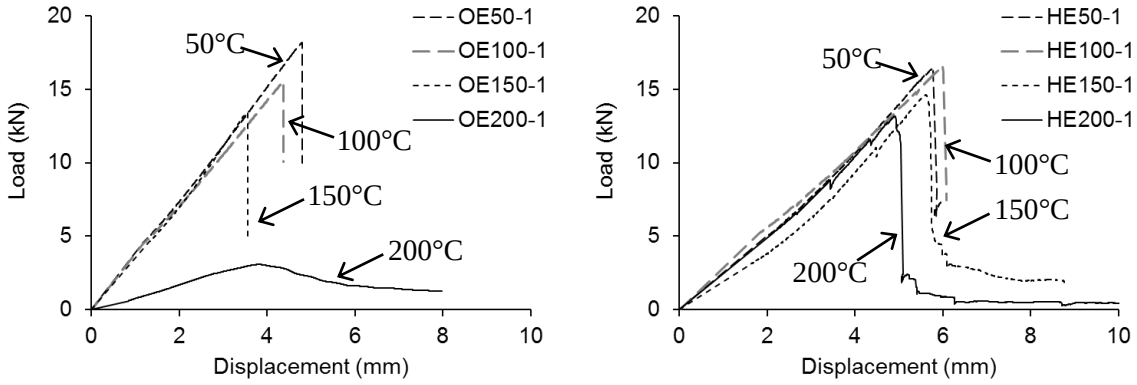

[1 kN = 0.225 kip; 1mm = 0.0394 in; °F = (°C × 1.8) + 32]

Fig. I.9 Load-displacemnt of interface test specimen: (a) bonded with ordinary epoxy, (b) bonded with high-temperature epoxy

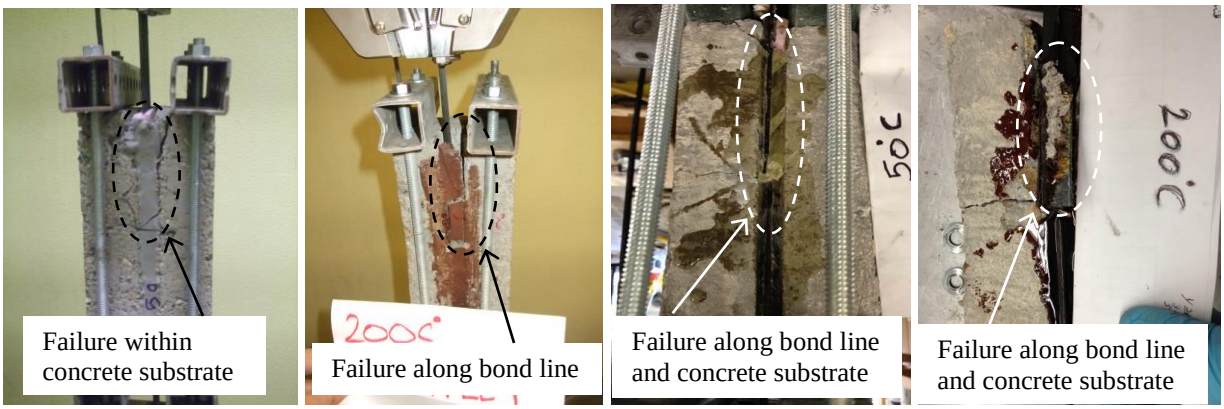

Fig. I.10 Failure mode: (a) ordinary epoxy at 50°C [122°F], (b) ordinary epoxy at 200°C [392°F], (c) high-temperature epoxy at 50°C [122°F], (d) high-temperature epoxy at 200°C [392°F]

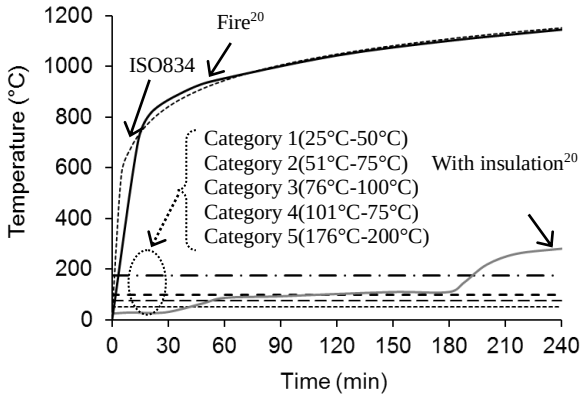

[°F = (°C × 1.8) + 32]

Fig. I.11 Effect of insulation and proposed design categories

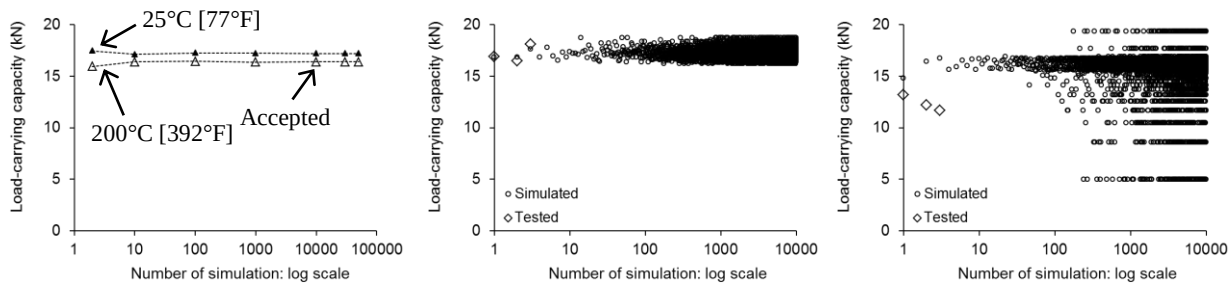

[1 kN = 0.225 kip]

Fig. I.12 Monte-Carlo simulation of HE category: (a) sensitivity analysis, (b) random sampling at 25°C [77°F], (c) random sampling at 200°C [392°F]

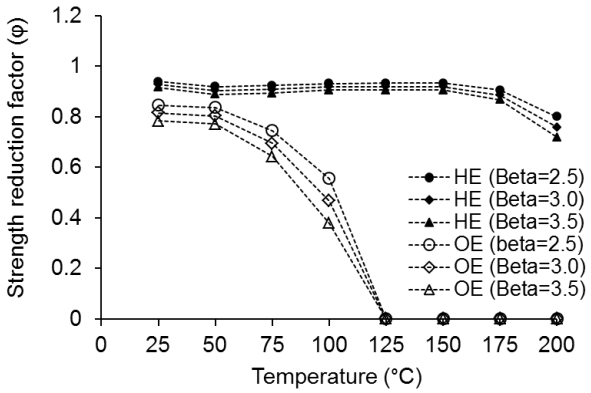

Fig. I.13 Variation of strength resistance factor

PART II. THERMOMECHANICAL BEHAVIOR OF NSM CFRP-CONCRETE INTERFACE

8. INTRODUCTION

Carbon fiber reinforced polymer (CFRP) composites frequently are used for strengthening existing structures. The load-bearing capacity of a concrete member is enhanced by bonding CFRP sheets/laminates with an adhesive. The range of application is broad from buildings to bridges. CFRP-strengthening is regarded as a cost-effective solution from a long-term standpoint because the non-corrosive material is durable and hence requires minimal maintenance costs.[1,2] A technique called near-surface-mounted (NSM) CFRP is an alternative retrofit technique of conventional externally-bonded (EB) CFRP. The NSM strengthening method is implemented in such a way that CFRP strips or rods are positioned inside the host structure along which narrow grooves are precut and permanently bonded. The performance of NSM CFRP is known to be better than that of EB CFRP in terms of enhanced bond, efficient use of material strength, ductility, surface preparation, environmental resistance, and vandalism.[3,4]

The occurrence of a fire must be taken into consideration when a building is retrofitted, while practitioners may have a concern about the use of CFRP because of its vulnerability to thermal load. A technical forum on the needs for FRP-research specifically pointed out this critical fact and stated that fire issues for strengthened structures are one of the priorities to advance to state-of-the-art.[5] A comprehensive understanding of thermomechanical distress and its consequences are in an early stage for CFRP-strengthened concrete members.[6] The effectiveness of CFRP-strengthening is degraded when subjected to thermal distress because the polymer-based binder of the CFRP and the bonding agent securing position of the CFRP are susceptible to temperature. Stringent assessment is imperative prior to recommending CFRP technologies to end-user sector. The majority of fire research for CFRP-strengthened members is concerned with EB CFRP,[7] whereas limited effort has been made for NSM CFRP techniques with a few technical papers being recently published. Kodur and Yu[4] carried out a numerical study on the behavior of reinforced concrete beams strengthened with NSM CFRP exposed to elevated temperatures. Emphasis was placed on temperature-dependent material properties, refined boundary conditions, and bond-deterioration issues. NSM CFRP-strengthened beams demonstrated higher temperature resistance compared to EB CFRP-strengthened counterparts. The location of NSM CFRP influenced thermal response of the strengthened beams. Palmieri et al.[8] reported the fire endurance and residual strength of concrete beams strengthened with NSM CFRP rods. Thermocouple wires were positioned at various locations inside and outside the strengthened beams to monitor temperature gradients. After one hour of fire exposure in a furnace, a maximum temperature of 130°C [266°F] was recorded at the level of the epoxy-bonded NSM CFRP due to the contribution of insulation layers (calcium silicate protection boards). No premature CFRP failure was observed. Firmo et al.[9] tested concrete prisms connected with NSM CFRP strips to examine bond performance of the interface at high temperatures up to 150°C [302°F], including a comparative study with EB CFRP application. Two types of bonding agents were used: epoxy and cementitious grout. The effective length of the NSM CFRP and the stiffness of the bond-slip behavior were a function of temperature. The bond strength of the NSM specimens was greater than that of the EB ones at all temperatures by a factor of 1.9 to 2.8. The

temperature-induced softening of the epoxy-bonded interface caused stiffness alteration, while considerable scatter was noticed.

This paper discusses the integrity of NSM CFRP-concrete interface subjected to thermomechanical distress (i.e., thermal and mechanical loads are applied simultaneously) with the following research subjects: material-level thermal relaxation, interfacial responses, and performance characterization. Previous studies illustrate that the failure of NSM CFRP is localized in the vicinity of the groove.[10] Therefore, the present experimental investigation focuses on behavior of an isolated effective stress zone, devoted to the CFRP-concrete interface, rather than that of structural members. Provided that CFRP-strengthened structures can achieve a fire rating of four hours when insulated and the temperature inside the insulation is typically less than 200°C [392°F],[11,12] a temperature range from 25°C [77°F] to 200°C [392°F] was adopted for this research program, assuming that the CFRP-concrete interface is insulated appropriately.

9. RESEARCH SIGNIFICANCE

Although recent technical findings report that the capacity degradation of CFRP-strengthened concrete members is apparent at elevated temperatures, such an effect is not fully characterized. Among many important aspects associated with CFRP systems in a fire, the interfacial behavior of CFRP bonded to a structure's substrate can be considered to be salient because interface deterioration affects the efficacy of CFRP-strengthening to a large extent. The significance of temperature-related research in CFRP application can be found in the ACI.440.2R-08 document:[13] the contribution of CFRP to the structural resistance of a strengthened member in a fire should be disregarded, and further research is required to elucidate the thermal behavior of a CFRP-strengthening system.

10. EXPERIMENTAL PROGRAM

This experimental program was comprised of two phases to examine thermomechanical behavior of NSM CFRP-strengthened concrete members at material- and interface-levels. This section briefs material details, specimen preparation, instrumentation, and test procedures.

10.1 Materials

A two-part low-viscous epoxy adhesive, consisting of a resin and a hardener to be mixed at a ratio of 3:1 by volume, was used for bonding CFRP strips to concrete. The manufacturer's datasheet states that the adhesive requires a minimum of seven days curing to achieve a tensile strength of 55 MPa [8,000 psi] with an elastic modulus of 3 GPa [440 ksi], including a glass transition temperature of 71°C [163°F]. Unidirectional CFRP strips (16 mm [0.63 in] wide × 2 mm [0.08 in] thick, each) have a tensile strength of 2,068 MPa (300 ksi) and a modulus of 124 GPa (18,000 ksi) at a failure strain of 1.7%. The strip's surface was textured by the manufacturer to enhance bond when interacting with the adhesive. Concrete was mixed in the laboratory with a specified concrete strength of 30 MPa [4,350 psi], while cylinder testing (ϕ 100 mm [4 in] × 200 mm [8 in]) based on ASTM C39 (*Standard test method for compressive strength of cylindrical concrete specimens*)[14] indicated an average strength of 30.4 MPa [4,408 psi] with a standard deviation of 2.9 MPa [421 psi].

10.2 Specimens

For material-level investigations (Fig. II.1), dog-bone coupons (12.2 mm [0.48 in] wide × 6.7 mm [0.26 in] thick × 100 mm [4 in] long) were prepared using the low-viscous epoxy adhesive and cured for seven days. CFRP-concrete assemblies were made to examine interface-level behavior at elevated temperatures. Each concrete block had dimensions of 100 mm [4 in] wide × 75 mm [3 in] deep × 150 mm [6 in] long, including a groove (12.5 mm [0.5 in] wide × 25 mm [1 in] deep × 150 mm [6 in] long) along the block, as shown in Fig. II.2(a). The groove configuration was designed in accordance with requirements of ACI440.2R-08[13,] and a precut styrofoam layer was used for shaping when casting concrete. Upon adequate curing of the concrete blocks, the surface along the groove was cleansed with a steel brush and a high-pressure air gun to eliminate weak oxidized cement particles so the epoxy adhesive could better bond to the concrete substrate. The groove was filled with the mixed epoxy, and CFRP strip was then inserted. It should be noted that the CFRP-concrete interface at the loading-end was intentionally unbonded to avoid stress concentrations when mechanically loaded. The assembled interface specimens were cured for at least seven days to warrant full strength of the adhesive as recommended by the manufacturer.

10.3 Test Setup and Thermal Exposure

The prepared material coupons were positioned to a 90 kN [20 kip] capacity hydroservo universal testing machine, as shown in Figs. II.1(b). A custom-made pull-out loading fixture was fabricated to test the interface specimens [Fig. II.2(b)]. Fabrication consisted of steel plates (t = 13 mm [0.5 in]) and high-strength threaded rods (10 mm [0.38 in] in diameter), which were snug-tight using nuts. To avoid premature slip failure of test specimens, a grip length of at least

25 mm [1 in] was provided. A temperature range from 25°C [77°F] to 200°C [392°F] was considered in this experimental research, provided that insulated structural members typically are exposed to such a temperature range when a fire takes place as mentioned earlier. To substantiate the planned elevated temperatures, electric heating pads were employed. The pad is made of perfluoroalkoxy (PFA) lead wires embedded in fiber glass reinforced silicone rubber, including a heating capacity up to 260°C [500°F]. Pads were directly contacted to the surface of interest for every specimen and thermocouple wires were installed to measure temperatures. For applying elevated temperatures to the adhesive and CFRP coupons, two heating pads were attached to both sides of each specimen [Fig. II.1(c)] and were clipped together to cover exposed areas of the specimen outside the gripping region. A similar heat-up plan was used for the interface test specimens, as shown in Fig. II.2(c). The concrete block side that had the CFRP-bond was covered because the other side was outside the interest of the current test program.

10.4 Thermal and Mechanical Loading Schemes

10.4.1 Material-level test

Thermal relaxation tests were conducted with epoxy coupons. A tension load of 1 kN [0.225 kips] was applied to individual coupons and held for thermal loading from 25°C [77°F] to 200°C [392°F] at a typical interval of 25°C [77°F]. Such a load level was equivalent to about 25% of the tensile capacity of the adhesive, which can represent a typical service condition. Three coupons were repeatedly tested per temperature. A reduction in tensile stress of the heated coupons was recorded with time, using a built-in load cell, until stress decreased to zero. Thermomechanical resistance of the adhesive subjected to temperatures higher than its glass transition temperature (71°C [163°F]) was insignificant according to preliminary monotonic tension tests conducted prior to carrying out the thermal relaxation test. Temperature-dependent CFRP properties were not examined since CFRP composites can retain their tensile capacity over 1,000°C [1,832°F] due to the contribution of carbon fibers[15] (Rostasy 1992), even though resins are thermally damaged.

10.4.2 Interface-level test

Two distinct mechanical loading plans (monotonic and cyclic) were designed to characterize behavior of the NSM CFRP-concrete interface when exposed to thermal distress: 25°C [77°F] to 200°C [392°F]. Two thermocouple wires were installed [Fig. II.2(a)] to measure heat conduction across the NSM CFRP interface. As shown in Fig. II.2(c), a heating pad (150 mm × 100 mm [6 in × 4 in]) was attached to the CFRP-strengthened side of the specimen and preheated at predefined elevated temperatures for five minutes. A monotonic tension load was then applied at a rate of 0.5 mm per minute, while the temperature was maintained until failure occurred. The test environment of the cyclic mechanical loading protocol was analogous to that of the monotonic counterpart, except that loading and unloading schemes were repeated from 10%P_u to 100%P_u at an interval of 10%P_u until the interface failed, in which P_u is the average ultimate load of the monotonically loaded interface specimens at a specific temperature. All load, displacement, and temperature values were recorded by a computerized data acquisition system.

11. TEST RESULTS

The thermomechanical behavior of the adhesive and the NSM CFRP-concrete interface is discussed in subsequent sections, including load-carrying capacity, thermal relaxation, failure mode, and thermal hysteresis.

11.1 Material-level Test

11.1.1 Thermal relaxation

Table II.1 reveals the effect of elevated temperatures on the variation of a stress-decrease rate for epoxy adhesive. The decrease rate was obtained between 20% and 70% of the maximum and minimum post-peak stresses (Fig. II.3). The control specimens at 25°C [77°F] exhibited insignificant stress-decrease rates, 0.004 MPa/sec [0.64 psi/sec] on average, therefore, the loading was terminated at 350 seconds [Fig. II.3(a)]. Thermal relaxation of the adhesive became obvious for the specimens subjected to 50°C [122°F], as shown in Fig. II.3(a), including an average stress-decrease rate of 0.029 MPa/sec [4.24 psi/sec]. When the applied temperature exceeded glass transition temperature of the adhesive (71°C [160°F]), the stress-decrease response time was noticeably reduced. For example, specimens exposed to 75°C [167°F] spent approximately 200 seconds [Fig. II.3(b)] before reaching zero stress from 12 MPa [1,740 psi], with an average stress-decrease rate of 0.082 MPa/sec [11.94 psi/sec]. As an exposure temperature increased, average stress-decrease rate augmented up to 0.221 MPa/sec [32.05 psi/sec] at 200°C [392°F], as listed in Table II.1. These observations indicate that stress transfer between the CFRP and concrete substrate is considerably influenced by thermal relaxation of the adhesive, which must be taken into account when insulation design is conducted for CFRP-strengthened members. Figure II.4 illustrates a relationship between the stress-decrease rate and temperature exposure. According to the fitted curve shown in Fig. II.4, stress-decrease rate gradually increased up to 75°C [167°F], beyond which an almost linearly-increasing trend was noticed.

11.2 Interface-level Test

11.2.1 Thermal conduction

Figure II.5 shows temperature variation measured by thermocouples 1 and 2 at the heated surface and beyond the interface, respectively. Although some scatter was noticed at the intersection between the heating pad and specimen surface [Fig. II.5(a)], the predefined nominal temperatures were maintained until the interface failed by mechanical load. The CFRP-strengthening system temperature gradually increased with time, as shown in Fig. II.5(b). Temperature transfer across the interface was not significant up to an applied temperature of 150°C [302°F], at which a maximum temperature of 37°C [99°F] was measured by thermocouple 2. On the other hand, a rapid increase in temperature transfer was observed for specimens subjected to 175°C [347°F] and 200°C [392°F], yet their temperatures were still lower than the glass transition temperature of the adhesive [Fig. II.5(b)]. This fact implies that heat transfer across the NSM CFRP-interface has discrete temperature boundaries rather than simple proportionality with temperature. The time-dependent heat current response of the interface is

given in Fig. II.6(a), including three specimens per temperature. The heat current (H) is defined as:

$$H = k_c A \frac{T_1 - T_2}{L} \tag{II.1}$$

where k_c is the composite thermal conductivity for the NSM CFRP interface; A is the surface area along the interface where heat is transferred (thermal contact); T_1 and T_2 are the temperatures measured by thermocouples 1 and 2 [Fig. II.2(a)], respectively; and L is the heat transfer length between thermocouples 1 and 2. To calculate composite thermal conductivity k_c, the rule of mixtures was used with an area fracture ratio of 15.4% and 84.6% for the CFRP, and epoxy adhesive inside the groove [Fig. II.2(a)] with thermal conductivities of 0.865 W/m per °C [0.5 Btu/hr ft per °F] and 0.346 W/m per °C [0.2 Btu/hr ft per °F]:[16] k_c = 0.426 W/m per °C [0.246 Btu/hr ft per °F], respectively. Heat current of the specimens initially increased due to a relatively large gap in temperature between both ends of the interface (thermocouple 1 and thermocouple 2), whereas the current decreased in an almost linear manner with an increase in time (i.e,. decay in temperature difference between the two thermocouples). Therefore, the heat flow mechanism of the NSM CFRP-concrete interface was transient or in a non-steady state until mechanical failure occurred. It also is thought that steady-state conduction may not occur across the interface since adhesive material will degrade (i.e., polymeric disintegration causing bond failure) when thermal equilibrium is achieved at or higher than its glass transition temperature. The heat current rate of each interface specimen was calculated by taking starting and ending points of the descending branch in the heat current response [Fig. II.6(a)] and summarized in Fig. II.6(b). The heat current rate tended to decrease with an increase in temperature, which can be explained by how the propagation of heat energy accelerated when thermal contact temperature augmented. The fitted equation may be used for design and practice.

11.2.2 Load-carrying capacity

Figure II.7 depicts load-displacement behavior of selected interface specimens. Linear-like responses were observed for all specimens up to peak loads, while their post-peak behavior was affected by the degree of thermal exposure. Specimens tested at 25°C [77°F] demonstrated abrupt load drops immediately after peak loads were achieved [Fig. II.7(a)]; conversely, specimens exposed to higher temperatures revealed gradual load-softening [Fig. II.7(b) and (c)]. These observations can be attributed to the phase transition of the epoxy adhesive: the glassy state of the adhesive subjected to a temperature below its glass transition temperature was shifted to a rubbery state when the applied temperature exceeded the glass transition temperature, and a progressive energy release was noticed. The temperature-dependent interfacial capacity of the test specimens is shown in Fig. II.8(a). The average capacity was reasonably maintained up to a temperature of 75°C [167°F], followed by a significant reduction to an average capacity of 0.46 MPa [67 psi] at 200°C [392°F]. Standard deviation of the interfacial capacity generally decreased with an increase in temperature [Fig. II.8(b)]. This fact clarifies that the rubbery state of epoxy in the specimens exposed to temperatures higher than the glass transition temperature provided glutinous characteristics and stable failure conditions were available. The coefficient of variation (COV) of the interface specimens appeared to be almost constant, with an average value of 0.21, regardless of exposure temperature. Experimental results were further expanded to

propose design equations, based on Monte-Carlo simulation, which can complement the limited number of test observations. A total of 80,000 random samples (10,000 samples per temperature) were generated, based on the statistical properties acquired from the test (Fig. II.8), to simulate the interfacial capacity at elevated temperatures (25°C [77°F] to 200°C [392°F]), as shown in the inset of Fig. II.9(a). A normality test revealed that probability distribution of the interface was Gaussian [Fig. II.9(a)]. The simulated mean capacity of the interface at a certain temperature was normalized by that of the control interface at 25°C [77°F] to estimate a reduction in capacity [Fig. II.9(b)]. Regression analysis was carried out in three distinct performance regions (stable, transition, and decaying) observed in Fig. II.8(a) and the following equations were derived:

$$C = \begin{cases} -0.066 \ln(T) + 1.1955 & \text{for } 25°C \le T \le 75°C \quad \text{(II.2a)} \\ -2.086 \ln(T) + 9.9475 & \text{for } 75°C < T \le 100°C \quad \text{(II.3a)} \\ -0.421 \ln(T) + 2.3002 & \text{for } 100°C \le T \le 200°C \quad \text{(II.4a)} \end{cases}$$

$$C = \begin{cases} -0.090 \ln(T) + 1.3702 & \text{for } 77°F \le T \le 167°F \quad \text{(II.2b)} \\ -2.516 \ln(T) + 13.814 & \text{for } 167°F < T \le 212°F \quad \text{(II.3b)} \\ -0.476 \ln(T) + 2.9061 & \text{for } 100°F \le T \le 200°F \quad \text{(II.4b)} \end{cases}$$

where C is the temperature-dependent capacity reduction factor that could be multiplied by the interfacial capacity at 25°C [77°F].

11.2.3 Failure mode

Figure II.10 illustrates failure modes of the interface at various temperatures. The specimens exposed to 25°C [77°F] showed typical pull-out failure in the concrete cover [Fig. II.10(a)], indicating that adhesion strength of the epoxy was adequate. Such a failure mode is predominantly observed in reinforced concrete beams strengthened with NSM CFRP composites.[10] Specimens at 50°C [122°F] showed a failure mode similar to those at 25°C [77°F]. When the applied temperature exceeded glass transition temperature of the adhesive, the change to failure mode was noticeable, as shown in Fig. II.10(b), where interfacial failure took place between the concrete surface and the adhesive. With another increase in temperature, the failure plane of the interface was completely shifted toward the adhesive side [Fig. II.10(c) and (d)]. These observations show why interfacial capacity was reduced with temperature in Fig. II.8(a) and clarify changing the bond-slip behavior of the interface in Fig. II.7.

11.2.4 Thermomechanical hysteresis

Results of the cyclic load test are provided in Fig. II.11 (three specimens were tested per temperature as in the static cases, while only one representative behavior is shown for clarity). For comparison, the ordinate values indicating the level of applied load were normalized by the average interfacial capacity of the statically loaded specimens at a corresponding temperature. The specimen exposed to 25°C [77°F] exhibited gradual increases in load and displacement, as shown in Fig. II.11(a). It is interesting to note that the cyclically-loaded specimen at failure revealed more displacement than the monotonically-loaded ones [Fig. II.7(a)], which was attributed to hysteresis of the interfacial slip. Unlike the specimen at 25°C [77°F], those exposed to higher temperatures, such as 125°C [257°F] and 200°C [392°F] available in Fig. II.11(b) and

(c), respectively, demonstrated insignificant displacement accumulation until they failed. It is thought that degree of interaction between the CFRP strip and the concrete substrate became weaker with an increase in temperature and the interfacial slip occurred in the adhesive layer for the high-temperature specimens. This assertion is supported by the transition of failure mode shown in Fig. II.10 (from concrete side to adhesive side). Variation of residual capacity in cyclically-loaded specimens is summarized in Fig. II.12. The effect of cyclic load was obvious on decreasing strength of the interface.

12. CHARACTERIZATION OF THERMOMECHANICAL INTERFACE BEHAVIOR

Capacity of the NSM-CFRP interface affected by thermomechanical distress was characterized by the Weibull theory[17]linked with the probability of failure.

12.1 Determination of Weibull Parameters

Reduced interfacial capacity may be modeled using the two-parameter Weibull function defined in Eq. II. 5:

$$\frac{P(T)}{P_0} = Exp\left[-\left(\frac{P(T)}{S}\right)^{\beta}\right] \tag{II.5}$$

where $P(T)$ and P_0 are the interfacial capacity at temperature T and at the initial temperature (25°C [77°F]), respectively, and β and S are the shape and scale parameters of the interface, respectively. To obtain the β and S parameters, double logarithm can be taken:

$$\ln\left[-\ln\left(\frac{P(T)}{P_0}\right)\right] = \beta \ln P(T) - \beta \ln S \tag{II.6}$$

The simulated interfacial capacities shown in Fig. II.9 were used when determining Weibull parameters, rather than the limited test data, so that more generalized conclusions were anticipated. According to Fig. II.13, the characteristic parameters were attained as β = -1.364 and S = 3.118.

12.2 Probability of Failure

The probability of failure for the characterized NSM-CFRP interfacial capacity depending on extent of thermomechanical distress, $P_f(T)$, was inferred and based on the aforementioned Weibull distribution and the capacity reduction factors proposed in Eqs. II.2-4:

$$P_f(T) = 1 - Exp\left[-\left(\frac{CP_0}{3.118}\right)^{-1.364}\right] \tag{II.7}$$

As shown in Fig. II.14(a), the probability of failure exponentially increased with a decrease in interfacial capacity. A failure probability of 0.4 or below was maintained until the capacity was reduced to approximately 5 MPa [725 psi], which is 14% below the average simulated-capacity of the interface at 25°C [77°F]. The interfacial capacity at a failure probability of 0.5 was found to be 4 MPa [580 psi], equivalent to an exposure temperature between 75°C [167°F] and 100°C [257°F]. It is important to note that physical interpretation of the probability of failure is not intended to mean deterministic failure of the CFRP-concrete interface, but indicates the level of risk associated with thermal and mechanical loads being applied simultaneously from a probability standpoint. Figure II.14(b) depicts transition of probability distribution functions of

the interfacial capacity with temperature. A wide, probabilistic domain was predicted in a temperature range of 25°C [77°F] to 75°C [167°F]; however, distributions tended to exhibit sharp peaks at their most probable capacities as temperature level increased, which implies that only a tiny fraction of the probable capacity became available. The cumulative distribution functions shown in Fig. II.14(c) demonstrate performance cohort of the interface in terms of temperature exposure and corresponding rates of capacity-decaying.

13. SUMMARY AND CONCLUSIONS

This paper elaborated on thermomechanical behavior of NSM CFRP-concrete interface subjected to elevated temperatures ranging from 25°C [77°F] to 200°C [392°F]. The effect of temperature-induced distress was studied at material- and interface-levels, including thermal relaxation, heat conduction, load-carrying capacity, failure mode, and damage characterization using the two-parameter Weibull function. Synergetic deterioration of the interface by thermal and mechanical loads was characterized probabilistically. The following conclusions were made:

- Transfer of interfacial stresses between the CFRP and concrete were controlled by the thermal relaxation mechanism of the bonding agent. Response time of the stress-decrease rates dwindled when adhesive was exposed to a temperature higher than its glass transition temperature.
- The heat flow of the interface was transient, rather than steady-state, up to failure of the strengthening system, due to the thermomechanical load. The extent of thermal contact accelerated progression of heat energy and discrete temperature boundaries, and altered failure planes from the concrete side to the adhesive side.
- Phase transition of the adhesive, depending upon temperature exposure, controlled behavior of the interface in such a way that brittle responses were shifted to gradual load-softening. The temperature-dependent capacity reduction factor proposed may be used when implementing CFRP-strengthening for existing building members along with the design of insulation.
- The hysteresis of the interfacial slip was noticed primarily in the adhesive layer when loaded cyclically and the degree of interaction between the CFRP and the substrate was reduced with temperature.
- The characteristic parameters attained as part of the two-term Weibull function were recommended for predicting the capacity degradation of the CFRP-concrete interface exposed to elevated temperatures. An exponential-response relationship was found between the interfacial capacity and temperature exposure. The range of the most probable capacity noticeably decreased with an increase in temperature, particularly above 150°C [302°F].

14. REFERENCES

[1] Karbhari, V.M. and Seible, F 2000. Fiber reinforced composites- advanced materials for the reneal of civil infrastructure, Applied Composite Materials, 7, 95-124.

[2] Bank, L. 2006. Composites for construction: structural design with FRP materials. John Wiley & Sons, Hoboken, NJ.

[3] Seracino, R., Jones, N.M., Ali, M.S.M., Page, M.W., and Oehlers, D.J. 2007. Bond strength of near-surface mounted FRP strip-to-concrete joints, Journal of Composites for Construction, 11(4), 401-409.

[4] Kodur, V. and Yu, B. 2013. Evaluating the fire response of concrete beams strengthened with near-surface-mounted FRP reinforcement, Journal of Composites for Construction, 17(4), 517-529.

[5] Porter, M.X. and Harries, K. 2007. Future directions for research in FRP composites in concrete construction, Journal of Composites for Construction, 11(3), 252-257.

[6] Bisby, L. and Stratford, T. 2013. Design for fire of concrete elements strengthened or reinforced with fibre-reinforced polymer: state of the art and opportunities from performance-based approaches, Canadian Journal of Civil Engineering, 40, 1-10.

[7] Bisby, L.A., Green, M.F., and Kodur, V.K.R. 2005. Response to fire of concrete structures that incorporate FRP, Progress in Structural Engineering and Materials, 7, 136-149.

[8] Palmieri, A., Matthys, S., and Taerwe, L. 2013. Fire endurance and residual strength of insulated concrete beams strengthened with near-surface mounted reinforcement, Journal of Composites for Construction, 17(4), 454-462.

[9] Firmo, J.P., Correia, J.R., Pitta, D., Tiago, C., and Arruda, M.R.T. 2014. Bond behavior between near-surface-mounted CFRP strip and concrete at high temperatures, Journal of Composites for Construction, Article ID 04014071

[10] De Lorenzis, L. and Teng, J.G. 2007. Near-surface mounted FRP reinforcement: an emerging technique for strengthening structures, Composites Part B, 38, 119-143.

[11] Kodur, V.K.R., Bisby, L.A., and Green, M.F. 2007. Guidance for the design of FRP-strengthened concrete members exposed to fire, Journal of Fire Protection Engineering, 17(5), 5-26.

[12] Chowdhury, E.U., Bisby, L.A., Green, M.F., and Kodur, V.K.R. 2008. Residual behavior of fire-exposed reinforced concrete beams prestrengthened in flexure with fiber-reinforced polymer sheets, Journal of Composites for Construction, 12(1), 61-68.

[13] ACI. 2008. Guide for the design and construction of externally bonded FRP systems for strengthening concrete structures (ACI440.2R-08), American Concrete Institute Committee 440, Farmington Hills, MI.

[14] ASTM. 2014. Standard test method for compressive strength of cylindrical concrete specimens, West Conshohocken, PA.

[15] Rostasy, F. 1992. Fiber composite elements and techniques as non-metallic reinforcement of concrete, Brite project 4142/BREU-CT910515, Evaluation of Potential and Production Technologies of FRP, Technical Report Task 1.

[16] Mallick, P.K. 2008. Fiber-reinforced composites: materials, manufacturing, and design, CRC Press, Boca Raton, FL.

[17] Weibull, W. 1939. A statistical theory of the strength of materials, Proceedings of Royal Swedish Institute of Engineering Research, 151, 1-45.

Table II.1 Thermal relaxation test results

Temperature	Specimen	Stress decrease rate (MPa/sec [psi/sec])			
		Individual	Average	Standard deviation	Coefficient of variation
25°C [77°F]	EC25 I	0.005 [0.79]	0.004 [0.64]	0.002 [0.23]	0.364
	EC25 II	0.003 [0.37]			
	EC25 III	0.005 [0.76]			
50°C [122°F]	EC50 I	0.029 [4.17]	0.029 [4.24]	0.001 [0.20]	0.048
	EC50 II	0.031 [4.47]			
	EC50 III	0.028 [4.08]			
75°C [167°F]	EC75 I	0.082 [11.97]	0.082 [11.94]	0.006 [0.83]	0.069
	EC75 II	0.088 [12.75]			
	EC75 III	0.076 [11.10]			
100°C [212°F]	EC100 I	0.104 [15.12]	0.126 [18.32]	0.024 [3.55]	0.194
	EC100 II	0.122 [17.71]			
	EC100 III	0.153 [22.14]			
125°C [257°F]	EC125 I	0.168 [24.41]	0.168 [24.41]	0.007 [1.06]	0.039
	EC125 II	0.180 [26.08]			
	EC125 III	0.179 [26.01]			
150°C [302°F]	EC150 I	0.173 [25.14]	0.165 [23.92]	0.007 [1.06]	0.044
	EC150 II	0.161 [23.42]			
	EC150 III	0.160 [23.21]			
175°C [347°F]	EC175 I	0.199 [28.79]	0.217 [31.50]	0.020 [2.90]	0.090
	EC175 II	0.238 [34.46]			
	EC175 III	0.216 [31.26]			
200°C [392°F]	EC200 I	0.216 [31.35]	0.221 [32.05]	0.020 [2.90]	0.093
	EC200 II	0.203 [29.49]			
	EC200 III	0.243 [35.30]			

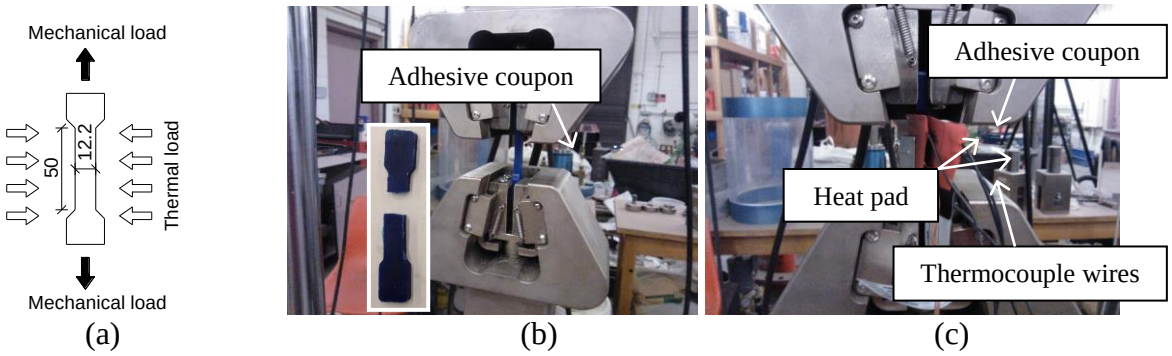

(a) (b) (c)

Fig. II.1 Thermal relaxation test for bonding agents: (a) coupons and loading scheme (unit in mm [1 mm = 0.0394 in]), (b) control adhesive, (b) heated adhesive

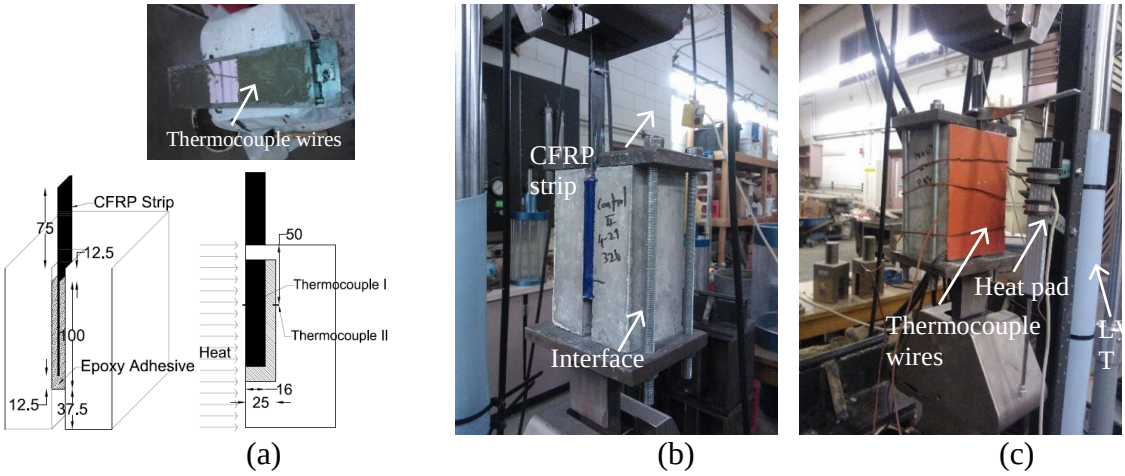

Fig. II.2 Thermomechanical test for NSM CFRP-concrete interface: (a) dimensions and thermocouple positioning (unit in mm [1 mm = 0.0394 in]), (b) control specimen, (c) heated specimen

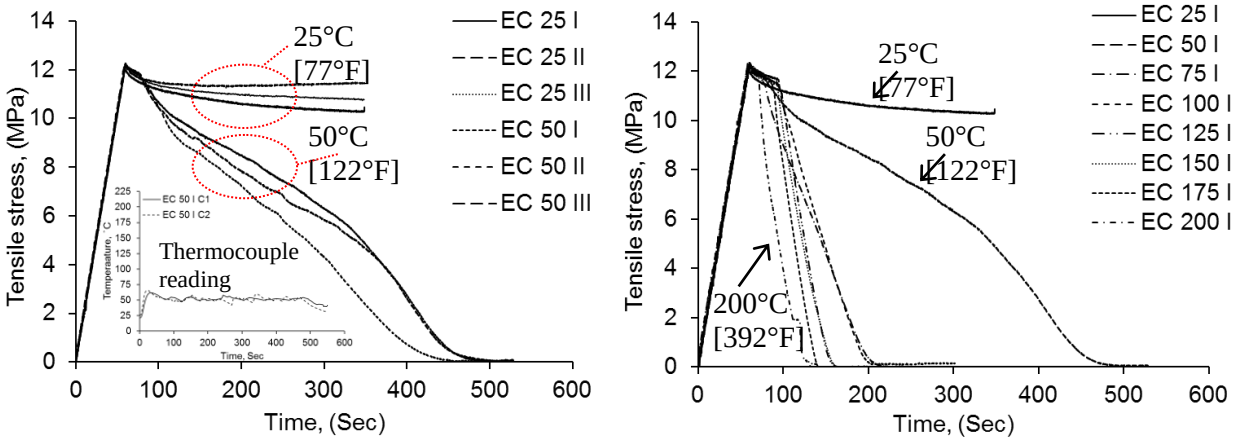

[1 MPa = 145 psi]

Fig. II.3 Thermal relaxation response of adhesives: (a) comparison between 25°C [77°F] and 50°C [122°F], (b) effect of elevated temperatures

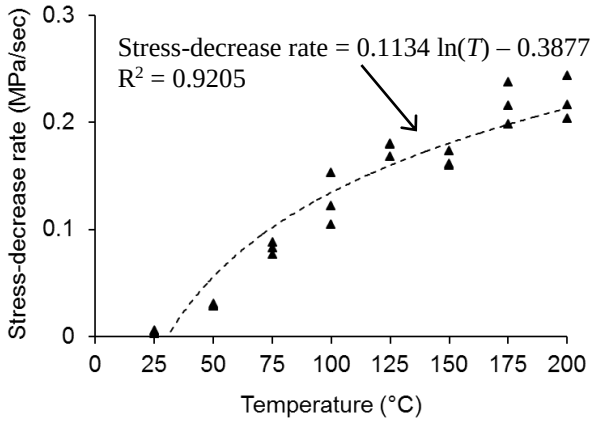

[1 MPa = 145 psi; °F = °C(9/5) + 32]

Fig. II.4 Stress decreasing rate due to thermal relaxation

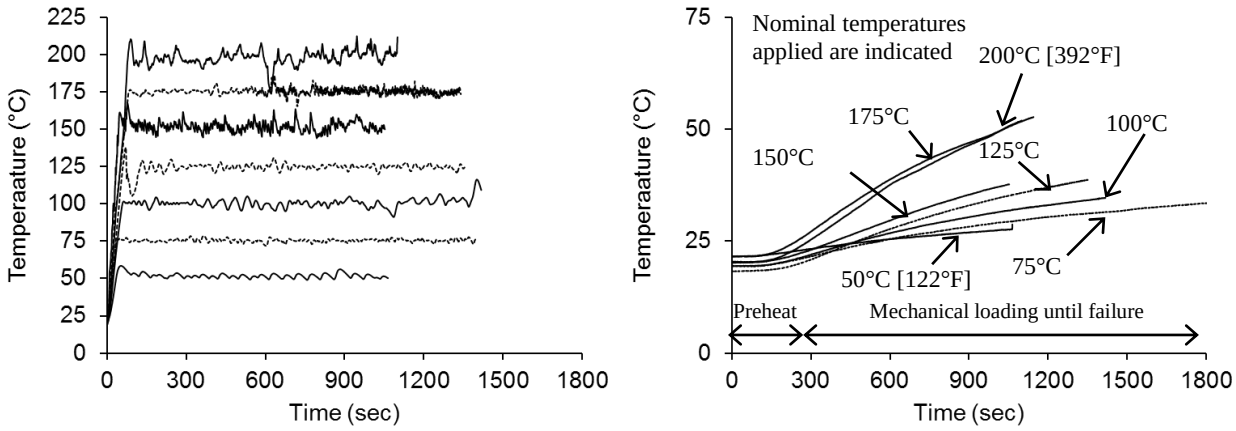

(a) (b)

[°F = °C(9/5) + 32]

Fig. II.5 Thermal conduction across the interface: (a) thermocouple 1 between the CFRP and heat pad, (b) thermocouple 2 between the adhesive and concrete

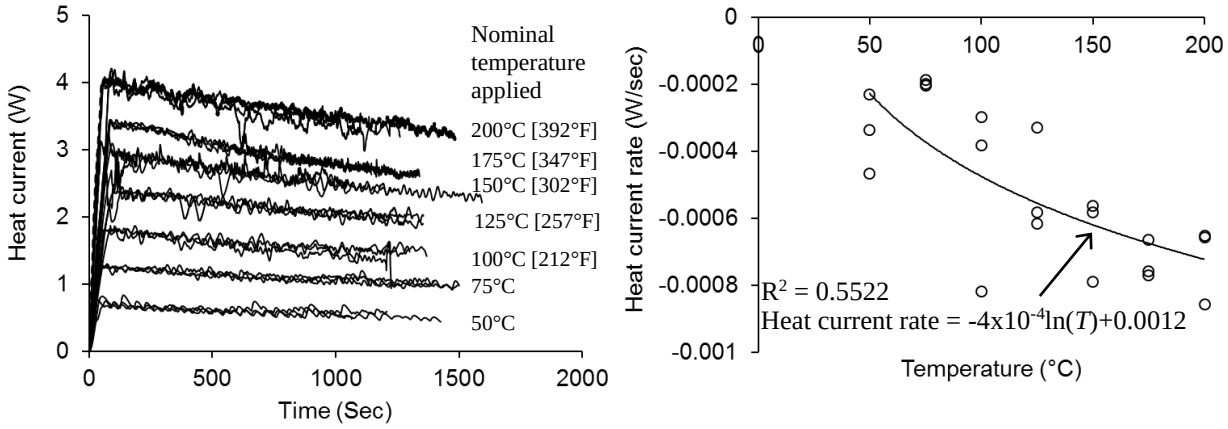

(a) (b)

[1W = 3.412 BTU/hr; °F = °C(9/5) + 32]

Fig. II.6 Variation of heat current in conduction: (a) heat current-time response, (b) heat current rate

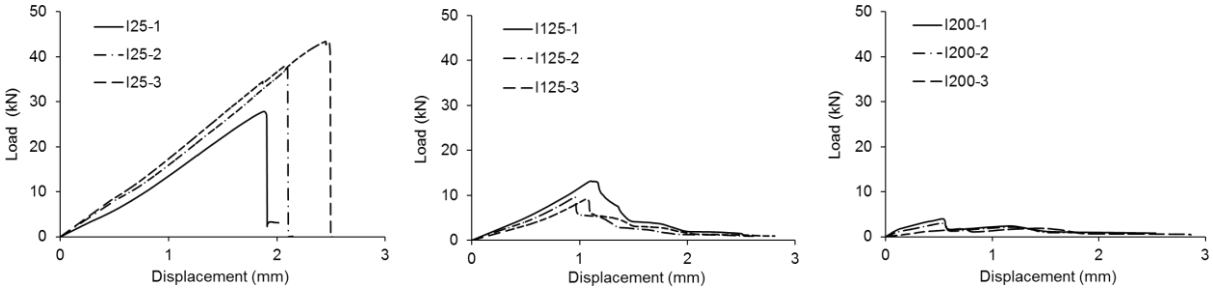

(a) (b) (c)

[1 kN = 0.225 kip; 1 mm = 0.0394 in]

Fig. II.7 Load-displacement behavior of interface specimens: (a) 25°C [77°F], (b) 125°C [257°F], (c) 200°C [392°F]

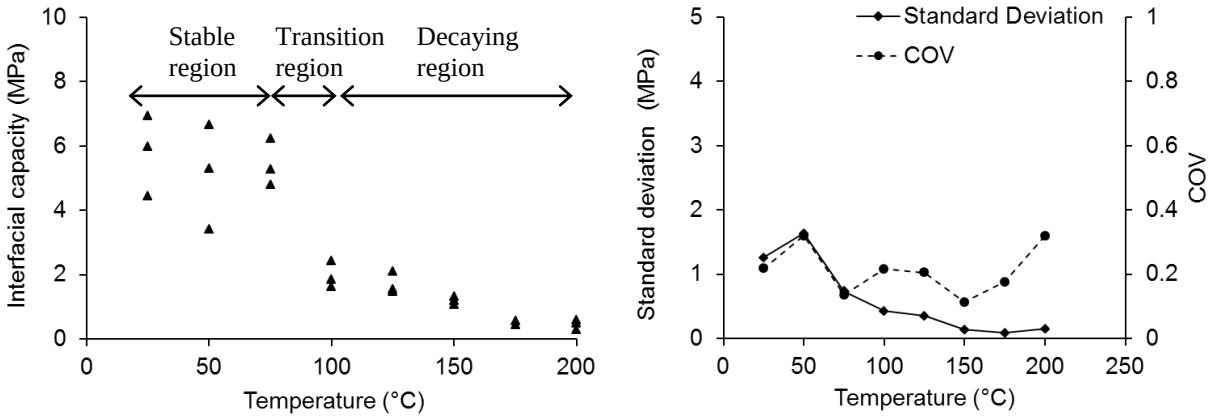

(a) (b)

[1 MPa = 145 psi; °F = °C(9/5) + 32]

Fig. II.8 Temperature-dependent interfacial capacity: (a) variation of bond stress, (b) statistical properties

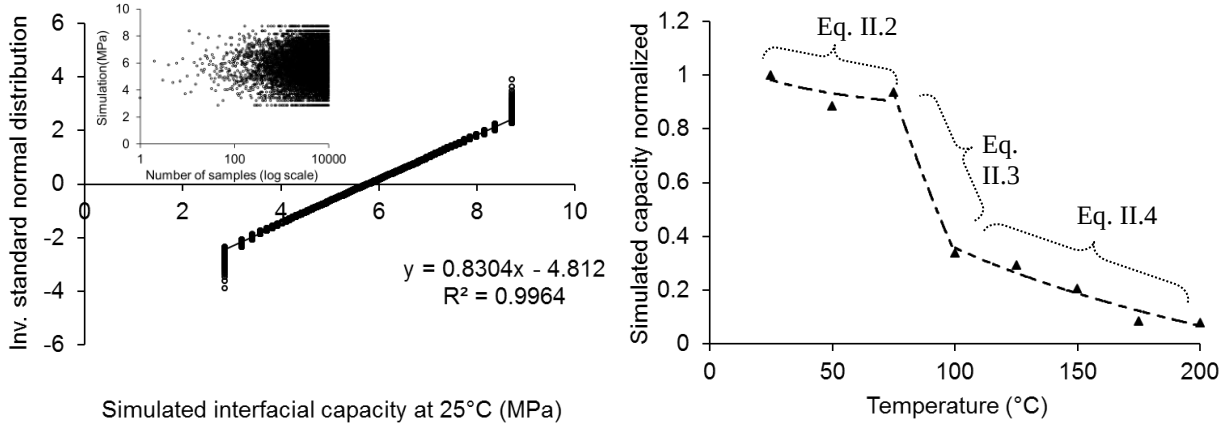

[°F = °C(9/5) + 32]

Fig. II.9 Simulated interfacial capacity and design proposal: (a) normality test and Monte-Carlo simulation, (b) capacity reduction due to temperature exposure

(a) (b) (c) (d)

Fig. II.10 Failure modes of the interface: (a) 25°C [77°F], (b) 75°C [167°F], (c) 125°C [257°F]; (d) 200°C [392°F]

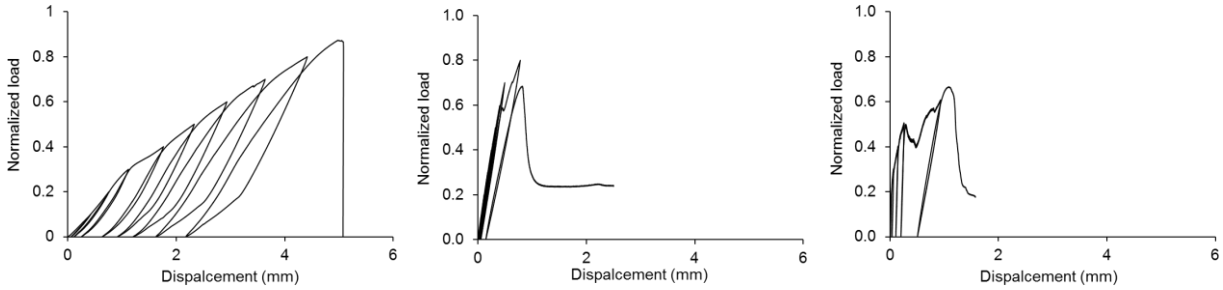

(a) (b) (c)

[1 mm = 0.0394 in]

Fig. II.11 Thermomechanical hysteresis: (a) normalized response at 25°C [77°F], (b) normalized response at 125°C [257°F], (c) normalized response at 200°C [392°F]

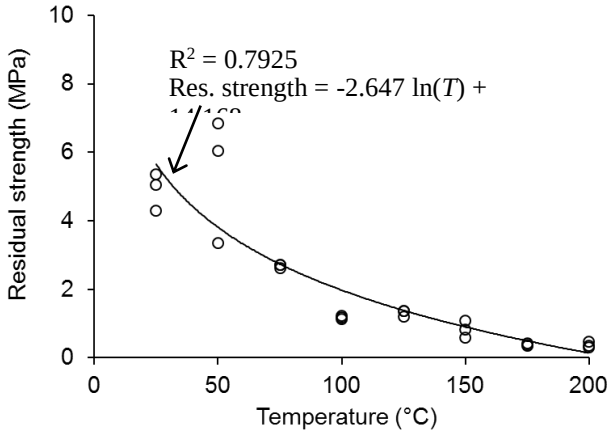

(a)

[1 kN = 0.225 kip; °F = °C(9/5) + 32]

Fig. II.12 Residual strength of cyclically loaded interface

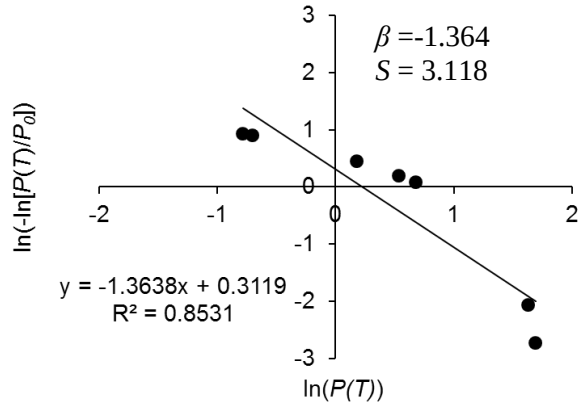

Fig. II.13 Determination of Weibull parameters

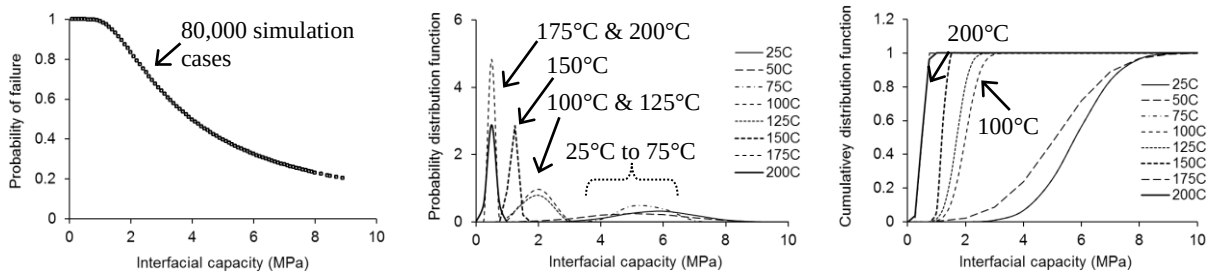

(a) (b) (c)

[1 MPa = 145 psi; °F = °C(9/5) + 32]

Fig. II.14 Predicted probability: (a) probability of failure, (b) probability distribution function, (c) cumulative distribution function